ABSTRACT

Title of dissertation: CYCLOTRON RESONANCE GAIN IN THE PRESENCE OF COLLISIONS

Nightvid F. Cole
Doctor of Philosophy, 2017

Dissertation directed by: Professor Thomas Antonsen
Institute for Research in Energy and Applied Physics

The conditions needed for the amplification of radiation by an ensemble of magnetized, relativistic electrons that are collisionally slowing down are investigated. The current study is aimed at extending the work of other researchers in developing solid-state sources of Terahertz radiation. The source type considered here is based on gyrotron-like dynamics of graphene electrons, or it can alternately be viewed as a solid state laser source that uses Landau levels as its band structure and is thus similar to a quantum cascade laser. Such sources are appealing because they offer the potential for a compact, tunable source of Terahertz radiation that could have commercial applications in scanning, communication, or energy transfer. An exploration is undertaken, using linear and nonlinear theories, of the conditions under which such sources might be viable, assuming realistic parameters. Classical physics is used, and the model involves electrons in monolayer graphene assumed to be pumped by a laser, follow classical laws of motion with the dissipation represented by a damping force term, and lose energy to the electromagnetic field as well. The

graphene is assumed to be in a homogeneous magnetic field, and is sandwiched between two partially-transmissive mirrors so that the device acts as an oscillator.

This thesis incorporates the results of two approaches to the study of the problem. In the first approach, a linear model is derived semi-analytically, which is relevant to the conditions under which there is gain in the device and thus stable operation is possible, versus the regime in which there is no net gain. In the second approach, a numerical simulation is employed to explore the nonlinear regime and saturation behavior of the oscillator. The simulation and the linear model both assume the same original equations of motion for the field and particles that interact self-consistently. The model used here is very simplified, but the aim here is to elucidate the basic principles and scaling behavior of such devices, not necessarily to calculate what the exact dynamics, outputs, and parameters of a fully commercially realized device will be.

Cyclotron resonance gain in the presence of collisions

by

Nightvid Cole

Dissertation submitted to the Faculty of the Graduate School of the
University of Maryland, College Park in partial fulfillment
of the requirements for the degree of
Doctor of Philosophy
2017

Advisory Committee:
Professor Thomas M. Antonsen, Chair/Advisor
Professor Edward Ott, Co-Advisor
Professor Mohammad Hafezi
Professor Thomas Murphy
Professor Wendell T. Hill

Motivation and Acknowledgments

The current project is intersectional among many fields. First and foremost, it is based on electrodynamics, which is the basis of how we model interactions between charged particles and static and dynamic electromagnetic fields. But it also can be looked at from a perspective of application - Terahertz radiation is a field which until recent decades has very little technology, engineering, or R&D to go along with it, because it occupied a "no man's land" between the optical domain which uses atoms and molecules as sources and detectors, and the RF domain, which uses electronic circuits and vacuum electronic devices (various wave tubes) as emitters and detectors.

As a physics graduate student, I have had interests in relativity and high-energy-density physics. Electrodynamics has always held a special appeal to me as a result of its intuitive nature (we can easily understand what an electric field is or a magnetic field is in terms of the force on a charge or current, but it is not similarly clear what a glue field is!)

I have my parents to be extremely thankful for. My interest in physics developed from a number of factors, without which I would almost certainly not be in the field. First, my father taught me extremely high-level mathematics in early childhood, and never told me I was too young to know something, if I asked, he answered. He also introduced me to computer programming when my age was still in the single digits. Second, both of my parents accepted my unusually nerdy interests, bought for me a number of "sciency toys", took me to science museums, and

even talked to my grade school teachers when it became clear that I was bored with the material being taught at grade-level. In my junior year of high school, I settled on physics as my final decision, and have no regrets on that choice. Third, both of my parents have always been there for me, in case any tough situations (academic or otherwise) came up in my life.

I have many others too numerous to mention, who have kept me company, offered me advice, been "study buddies", and kept me on track. I want to especially thank my former colleague, Shane Squires, for helping me when Matlab or LaTeX refused to work/compile and I had trouble figuring out what to do. He had an amazing ability to instinctively know what I was doing wrong and show me how to fix the problem. My anxiety evaporated when he was around. Eventually, I became more comfortable doing it on my own, and also my colleague Trystan Koch for an enormous amount of help with debugging Latex documents.

Other colleagues and friends who gave me important and useful advice along the way include Zhixin Lu, Jaideep Pathak, Benedict Mondal, Mark Herrera, Martin Mittendorff, Christopher Bambic, and many more.

And my committee members have all given me a lot of useful input along the way in too many ways to mention:

Thomas Antonsen (advisor)

Ed Ott (co-advisor)

Thomas Murphy

Mohammad Hafezi

Wendell T. Hill (dean's representative)

Table of Contents

Acknowledgments ii
Table of Contents iv
List of Figures v
Chapter 1: Introduction 1
Section 1 Graphene band structure 8
Section 2 Particle dynamics 10
Section 3 Electromagnetic field equations of motion and dynamics 13
Section 4 Necessity of electron inversion 17
Section 5 Chapters 2 and 3 overview 21
Chapter 2: Linear Theory 23
Section 1 THz gain 30
Section 2 Discussion 47
Section 3 Conclusion 53
Section 4 Acknowledgements 54
Section 5 Appendix: Semi-analytical treatment of integrals 54
Chapter 3: Nonlinear Theory 58
Section 1 Introduction 58
Section 2 Theory 63
Section 3 Numerical Simulation 71
Section 4 Conclusion 77
Section 5 Appendix: Intuitive Understanding of Gain 78
Bibliography 81

List of Figures

1.1 Basic band structure of undoped graphene near the Dirac point with the valence band (blue) filled and the conduction band (red) empty. The x and y axes represent the two components of electron momentum in the plane of the graphene, while the z axis represents the electron energy (zero point arbitrary). 8

1.2 Same as Figure 1.1, except the graphene is doped and possesses a bandgap. 9

1.3 Box representing a volume $L_x \times L_y \times L_z$. 15

1.4 Optically pumped graphene (black, pumping beam not shown) is sandwiched between two partially transmissive mirrors (green). In "forward wave only" mode, the beam is incident on the graphene (A). Beam then undergoes a gain due to the excited conduction electrons gyrating, and then undergoes an absorption by the graphene after this process (B). Beam is partially transmitted by a mirror (D) and partially reflected (C). Then the beam undergoes the same processes on the other side (E,F,A) and the cycle repeats itself. In "forward and backward wave" mode, half the THz energy is incident in the forward direction (A) while the other half is simultaneously incident on the graphene in the backward direction (C). 21

2.1 a) Schematic of graphene band structure showing valence electrons and electrons excited by a laser pulse with photon energy $2E$. b) Schematic of configuration analyzed showing orientation of graphene sheet, applied magnetic field, and incident and transmitted probe wave. © 2017 IEEE. 27

2.2 Normalized gain versus normalized frequency for several dimensionless slowing down times. For this plot the normalized half bandgap energy is $m'c'^2/E_i = \gamma_i^{-1} = 0.00585$. The solid portions of each curve indicate where $\cos(\phi_R + \pi/4) < 0$, where ϕ_R is defined in Eqs. (2.45) and (2.48). Diamonds and stars represent Landau transition energies for 3 T magnetic field, with the N = 10 (diamonds) and N = 5 cases (stars) arising at electron energies of 199 and 140 meV, respectively. g = Re(G-L) where G and L are defined by Eqs. (2.38) and (2.39), τ is the time scale of damping of electron motion, and the independent variables are explained by Eqs. (2.9), (2.40), (2.25), and (2.42). Amplification of the THz field cannot occur when g <0. © 2017 IEEE. 41

2.3 Normalized gain versus normalized frequency (same variables as in Fig. 2.2) for several values of normalized half band gap energy. The normalized slowing down time is $\omega_i\tau = 44.1$ for all curves shown. The curves represent 3 selected half-band-gap energies γ_i^{-1} (see Eq. (2.41)). The solid portions of each curve indicate where $cos(\phi_R + \pi/4) < 0$, where ϕ_R is defined in Eqs. (2.45) and (2.48). © 2017 IEEE. 44
2.4 Gain maximized over frequency as a function of slowing down time $\omega_i\tau$ and initial normalized half-bandgap γ_i^{-1}. © 2017 IEEE. 45
2.5 Dimensionless frequency at which the gain peaks in Fig. (2.3) and (2.4) occur. © 2017 IEEE. 46
2.6 Frequency and quantum index as a function of energy and magnetic field (log-log). Magenta square is 3 T magnetic field and 171 meV energy, the other two are 8 T field and 171 meV/500 meV (respectively). © 2017 IEEE. 47
2.7 Schematic of apparatus using mid-IR laser pumping. Partially transmissive curved mirrors (blue) form a cavity and contain a beam of THz radiation (green). This is amplified by the graphene (yellow-orange) which is pumped by mid-infrared radiation (gray wavy line) from a laser (not shown). The cavity is symmetric and gives two identical output beams (slightly darker green). 48

3.1 Dynamics: different slowing down times superimposed with the same ω_i. Inelastic scattering which acts as a variation in the slowing-down time τ still can allow gain to occur in frequency ranges where the gain is positive across the range of τ values. Here is an example of how this could be the case. In a narrow range of frequences between 10 and 12 THz, all the gain curves are positive for $\omega_i\tau$ values running from 27 to 42. 62
3.2 Gain, defined as the $G - L$ from Eq.(3.20), plotted vs. normalized frequency for linear model and numerical result for monochromatic field, single pass, and different electric field strengths expressed as a fraction of the critical field strength (see Eq. 3.27) for nonlinear behavior 74
3.3 Gain plotted vs. normalized frequency, zoomed in. Curves at same field strengths as in Fig. (3.2). 75
3.4 Efficiency ramp up, 288 passes 77
3.5 Dynamics:phase angle 78
3.6 Dynamics: complex exponential $e^{i\Delta\bar{\theta}(t)}$ versus time. Imaginary part excluded. 79
3.7 Dynamics: Integral of complex exponential. Imaginary part excluded. 80

Chapter 1: Introduction

In 1926 the idea of the cyclotron was invented at Aachen University. Electrons in a magnetic field experience a force that allows them to move in circles (gyrate) around the magnetic field lines (longitudinal motion along the field lines can also occur.) The angular velocity (in this writing SI units are used) is eB/m. If a rotating electromagnetic field is applied to the gyrating electrons at the same angular velocity, resonance occurs. Originally cyclotrons were designed as particle accelerators. In this mode of operation, the particles gain energy from the rotating field. The reverse may also occur, where the electrons lose energy by emitting cyclotron radiation.

The gyrotron is a modified form of the cyclotron that makes use of relativistic effects to make it possible to amplify radiation, thus functioning as a type of maser. The cyclotron formula is only valid for non relativistic electrons. In the relativistic case, (angular) frequency changes to $eB/(\gamma m)$. As with the cyclotron, electrons may gain or lose energy, depending on the relative phase of the electrons and the applied rotating field. Unlike for the cyclotron, however, relativistic effects allow electrons to phase-bunch ([1]). Under the right conditions the gyro-cyclotron, or gyrotron, becomes an oscillator, which self-seeds its own radiation and amplifies it, allowing it to become a high-powered microwave source.

The conventional gyrotron [2], also known as the cyclotron resonance maser, is a microwave source that makes use of stimulated cyclotron radiation. According to classical gyrotron theory, a gyrotron will produce radiation at the fundamental or a harmonic of the base angular velocity of gyration. For a particle of charge q and mass m at a relativistic factor $\gamma = (1 - v^2/c^2)^{-1/2}$ and in a uniform magnetic field of strength B, this is given by

$$\omega = \frac{|qB|}{\gamma m}. \tag{1.1}$$

For an electron with relativistic factor $\gamma = 1.1$, and $|B| = 2\text{T}$, this yields an output fundamental (cyclic) frequency of

$$\nu_g = \frac{\omega}{2\pi} \;=\; 50.8 \text{ GHz}. \tag{1.2}$$

Stimulated radiation is possible due to the relativistic energy dependence of the gyration frequency of an electron in a uniform magnetic field.

An additional condition usually required for cyclotron gain is that the electron distribution function be inverted; that is, the derivative of the distribution function with respect to energy should be positive ($\partial f/\partial E > 0$) for some range of energies. This condition is easily met in a conventional gyrotron, where electrons are injected into, travel through, and leave a cavity during a sufficiently short period of time that their distribution is not "thermalized" by collisions. A situation in which an inverted distribution function is not realized is one in which electrons are injected into an interaction region and slow down due to collisions before being removed. In this case, for reasonable models of the thermalization process, the distribution function

is a monotonically decreasing function of energy. We will find that even in this case, gain is present at some oscillation frequencies if the slowing down time is sufficiently long, and if correlations between instantaneous electron energy and electron "birth time" (equivalent to injection time) are not destroyed. To analyze this effect it is necessary to self-consistently treat the collisional and dynamic response of the electrons to the applied fields. This is in contrast to the customary approach where collisions may have a role in determining the unperturbed distribution function, but are then neglected or treated heuristically in determining the perturbed distribution function.

It is desired to produce radiation in the terahertz (THz) range without requiring extraordinarily high magnetic fields of several tens of Tesla, which are only available in expensive, large-scale, superconducting, or pulsed, electromagnets [3]. Lower fields produce frequencies only at 100 GHz or in some cases a few 100s of GHz. [4] This can be accomplished if the effective mass of the electron can be lowered by working with conduction band electrons of a solid material [5], while essentially retaining the principles of gyrotron physics. Consideration of a graphene-based gyrotron is a motivation for this paper. Electrons can be optically pumped from the valence band to the conduction band by an infrared laser, subsequently emit cyclotron radiation, and then eventually effectively removed by falling back into the valence band of the graphene. By contrast, in many traditional semiconductors, the band structure is more complex, and so is the emission spectrum from transitions between Landau levels (the quantum description of emission equivalent to cyclotron radiation). Band structure and emission spectra can be kept simple by

using Landau levels of a single species of charge carrier, and graphene can keep effective mass low enough to allow for magnetic fields available at $T \geq 77$ K to suffice. Light-to-heavy-hole lasing, one of the most plausible semiconductor alternatives for producing tunable far infrared oscillators, would require magnetic fields which might pose a problem for operation at $T \geq 77$ K, and germanium semiconductor-based cyclotron resonance maser (SCRM) sources, although otherwise promising, require even lower temperatures since only the lowest few Landau levels are involved [1] .

Previous work has focused on three broadly similar topics : One approach is to consider cyclotron resonance in graphene at low-lying Landau states that often must be treated quantum mechanically. The focus is on issues such as population inversion of Landau states in graphene [6], [7], and on graphene Landau lasing in the quantum regime [8], [9], [10]. The second approach is to study electron behavior in graphene in the absence of a magnetic field as a THz source. This includes THz gain in optically pumped graphene with no magnetic field [11], THz gain in graphene using dielectric substrates and photonic boundary conditions but no magnetic field [12], and femtosecond-scale transient population inversion in optically pumped graphene due to carrier cooling and Auger recombination but no magnetic field [13]. The third approach is to study conventional gyrotrons and other vacuum-electronics sources of THz radiation from electrons in a vacuum [14], [15]. Our approach is different from the first category because we consider the case of high quantum numbers that should be possible to approach using a classical treatment, different from the second category because we are using a magnetic field, and different from the third category because we are using graphene. Nonetheless, it has aspects in common with all three

previous approaches and could thus be considered an interdisciplinary combination.

As discussed in Ref. ([1]), another type of source involves solid-state devices. The behavior of electrons in a solid is not the same as in a vacuum, even if the other parameters of the problem, such as the applied magnetic field strength, are the same. This is true even in graphene, with electrons having a relatively long mean free path. One reason is that such systems are often necessary to describe using quantum-mechanical dynamics instead of using classical mechanics for gyrotron operation. While related to the classical laws, these dynamics are different. For one thing, the electrons in a solid are subject to the Pauli exclusion principle, which may provide an absolute minimum energy that they are physically able to have. Electrons are also sometimes accompanied by holes. Furthermore, quantum mechanics actually discretizes the permitted energy the electrons can have in a magnetic field. This is known as Landau quantization. The expressions regarding this quantization in graphene are given in Ref. ([16]), with the allowed energies given by (Ibid.)

$$E_n = sgn(n)\sqrt{2e\hbar v_F^2|n|B} + E_0, \tag{1.3}$$

where E_n is the energy associated with an electron in level number n, n is a numerical index for the energy level which may be positive, zero, or negative, e is the elementary charge, v_F is the Fermi speed (about 10^6 m/s in graphene), B is the magnetic field strength, and E_0 is a base or reference-point energy.

The highest energy level that is filled by electrons at absolute zero (when the system has its lowest overall energy) is known as the Fermi level. Excited electrons

can only lose energy until they get down to this level, due to the Pauli exclusion principle, unless they recombine with holes in the valence band - since holes are simply unfilled energy states below the Fermi level.

By varying the doping of the graphene, the Fermi level can be "tuned" so that all the negative-n states are filled at absolute zero, but the nonnegative-n states are not (Mittendorff, personal communication). This makes the interpretation of the electron motion easier, since the negative-n states are the ones with no classical analog.

The quantum mechanical approach has been used in a number of papers in the small-n regime (e.g. [8]). It is generally accepted in many fields of physics that quantum mechanics is necessary when the quantum numbers of the system are small, but when the quantum numbers are large, the *correspondence principle* states that classical mechanics should appear as a limiting case. Though quantum mechanics is always correct, there are practical reasons that classical physics is useful. First, classical mechanics is intuitive, and allows the motion to be described by particle trajectories that have an obvious interpretation. Second, classical mechanics is computationally easier than the quantum mechanics is, because quantum mechanics must consider all possible motions, even those that violate the classical equations of motion. One can of course come up with simplifying assumptions that make quantum calculations reasonable, such as the two-level approximation or various statistical approximations, but these are only good in the *deep quantum regime* where n is 0 or 1 only. Third, as will be seen, the classical model better elucidates the scaling properties of the system.

When incorporating scattering into a classical model, scattering cross sections for electrons, which are results of a quantum calculation, must be "put in by hand" to the dynamical equations. An effective theory can be built by noting that small-angle inelastic scattering events can be viewed as a "friction" on the electron. (Ultimately, of course, macroscopic friction is a consequence of microscopic scattering events, and must physically be some large-number limiting case of microscopic scattering dynamics.) The model described in this thesis treats the "friction" on the electron as a classical force opposing its motion of the form $\dot{p}_{fr} = -p/\tau$, where τ is a time constant which shall be called the "damping time". For these reasons, the analysis here takes advantage of the correspondence principle, and is classical, not quantum, in nature.

Though it would be interesting to explore the classical-quantum correspondence in this context in more detail, that matter is beyond the scope of this thesis. Instead, the focus will simply be on the classical dynamics of what is effectively a solid-state analog of the gyrotron, operating as an oscillator at terahertz (THz) or far infrared (FIR) frequencies.

The present model assumes that the magnetic field is perpendicular to the plane of the graphene, and that the THz radiation being amplified is travelling normally through the graphene and is circularly polarized. The graphene is pumped by an infrared laser.

1.1 Graphene band structure

Undoped graphene has the Dirac band structure [17], equivalent to ultrarelativistic ($\gamma \gg 1$) (or massless) electrons, with a band velocity of 10^6 m/s. The conduction band and the valence band are touching at the Dirac point (see Fig. 1)

.

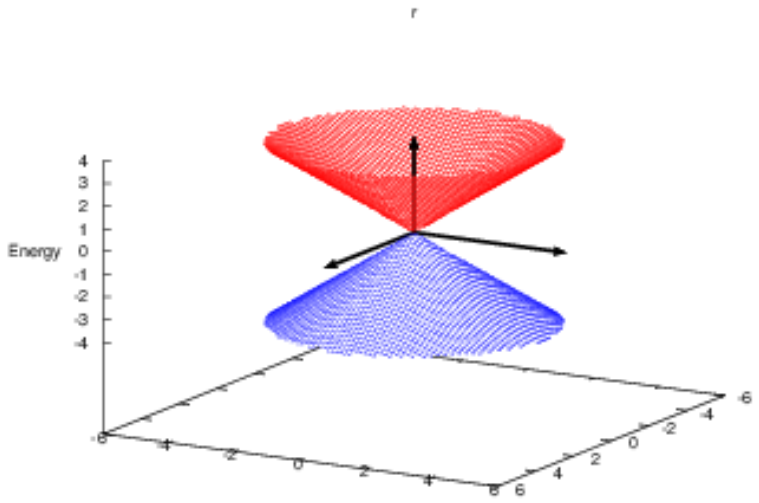

Fig. 1.1: Basic band structure of undoped graphene near the Dirac point with the valence band (blue) filled and the conduction band (red) empty. The x and y axes represent the two components of electron momentum in the plane of the graphene, while the z axis represents the electron energy (zero point arbitrary).

The energy-momentum dispersion relation for this (massless) band structure is

$$E = pc', \tag{1.4}$$

where c' is the band velocity (Fermi velocity).

Although this allows for gyrotron-like action in an applied static, homogeneous magnetic field perpendicular to the graphene sheet plane, the efficiency will be low. This is because of the ultra-relativistic nature of the band structure. (In conventional gyrotrons the efficiency is highest when the electrons are weakly relativistic with kinetic energies up to 80 keV [18].) Doping the graphene allows for an alteration of the band structure, in agreement with theoretical predictions for bilayer graphene [19]. (Also see Fig. 1.2)

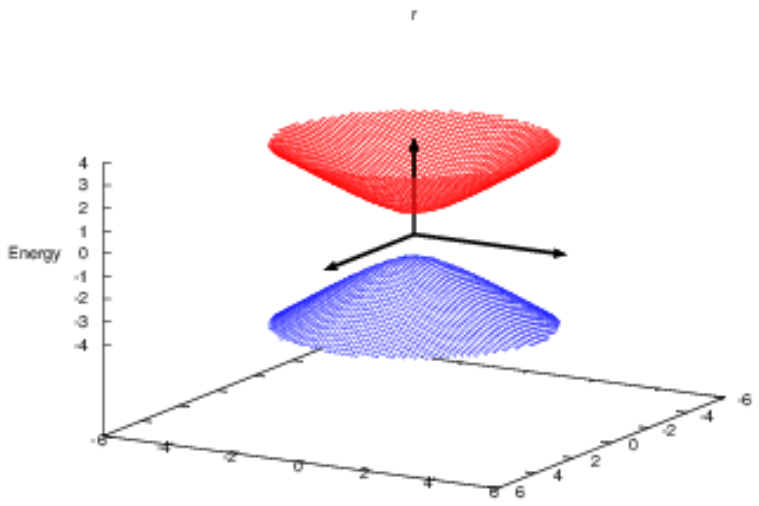

Fig. 1.2: Same as Figure 1.1, except the graphene is doped and possesses a bandgap.

In doped graphene with a small band gap, the band structure is hyperbolic, so the relation between energy and momentum of a (conduction band) electron is given

by the quasi-relativistic expression (see Linear Theory section for more detail):

$$E = \sqrt{(pc')^2 + (m'c'^2)^2}, \tag{1.5}$$

where $c' = v_{_F}$ is the Fermi speed mentioned earlier, and m' is the effective mass. The band gap is $2m'c'^2$.

The electron's classical velocity is given by

$$v = \frac{dE}{dp} = \frac{pc'^2}{E} = \frac{p}{m'\gamma'}, \tag{1.6}$$

where

$$\gamma' \equiv \frac{E}{m'c'^2} = \sqrt{1 + \left(\frac{p}{m'c'}\right)^2}. \tag{1.7}$$

1.2 Particle dynamics

The i^{th} electron at time t has a momentum $\mathbf{p}(i,t)$ which may be expressed in Cartesian coordinates as

$$\mathbf{p}(i,t) = p_x(i,t)\hat{x} + p_y(i,t)\hat{y}. \tag{1.8}$$

Introducing polar coordinates $p(i,t)$ and $\theta(i,t)$, this becomes

$$\mathbf{p}(i,t) = p(i,t)[\cos\theta(i,t)\hat{x} + \sin\theta(i,t)\hat{y}]. \tag{1.9}$$

Differentiating the latter with respect to time, and using the Lorentz force relation $\dot{\mathbf{p}} = q\big[\mathbf{E} + \mathbf{v} \times \mathbf{B}\big]$, and the velocity expression $\mathbf{v}(t) = \mathbf{p}(t)/(\gamma(t)m')$, we obtain the pair of equations

$$\dot{p} = -e[E_x \cos\theta + E_y \sin\theta], \tag{1.10}$$

and

$$p\dot{\theta} = -e[-E_x \sin\theta + E_y \cos\theta] + p\frac{\omega_{_L}}{\gamma'}, \tag{1.11}$$

where

$$\omega_{_L} \equiv \frac{eB}{m'}. \tag{1.12}$$

The above, however, apply only to an idealized case with no scattering of electrons by phonons or inhomogeneities/defects in the graphene. Both elastic and inelastic scattering can occur. A simple model which treats inelastic scattering events of primarily small, longitudinal momentum transfers as an overall damping on the electron momentum causing it to decay exponentially with time constant τ can be used. In this case, the equation for $\dot{p}$ becomes

$$\dot{p} = -e[E_x \cos\theta + E_y \sin\theta] - \frac{p}{\tau}, \tag{1.13}$$

while that for $\dot{\theta}$ is now

$$\dot{\theta} = -p^{-1}e[-E_x \sin\theta + E_y \cos\theta] + \frac{\omega_{_L}}{\gamma'}. \tag{1.14}$$

Now we transform to a rotating frame with angular velocity ω and initial phase ϕ_0. This involves transforming both the particle momentum and the field. The

transformed field is parameterized as perpendicular and parallel field components ($E_\parallel(t)$ and $E_\perp(t)$), as experienced by the electrons (Some variables have implicit indices i, t with i suppressed):

$$\begin{pmatrix} E_x(t) \\ E_y(t) \end{pmatrix} = \begin{pmatrix} \cos(\omega t + \phi_0) & -\sin(\omega t + \phi_0) \\ \sin(\omega t + \phi_0) & \cos(\omega t + \phi_0) \end{pmatrix} \begin{pmatrix} E_\parallel(t) \\ E_\perp(t) \end{pmatrix}. \tag{1.15}$$

The transformed particle momentum has magnitude $p(i,t)$ (which is unchanged by the transformation), and angle $\overline{\theta}(i,t) \equiv \theta(i,t) - \omega t - \phi_0$. With the field now expressed in terms of $E_\parallel(t)$ and $E_\perp(t)$ and the particle momentum expressed in terms of $p(i,t)$ and $\overline{\theta}(i,t)$, the equations of motion become (indices i, t suppressed):

$$\begin{gathered} \dot{p} = -e[\cos\overline{\theta}E_\parallel + \sin\overline{\theta}E_\perp] - \tfrac{p}{\tau}, \\ and \qquad , \\ \dot{\overline{\theta}} = -\omega + \dot{\theta} = -\omega + \tfrac{\omega_L}{\gamma'} - p^{-1}e[-\sin\overline{\theta}E_\parallel + \cos\overline{\theta}E_\perp] \end{gathered} \tag{1.16}$$

which are the rotating-frame electron equations of motion. To simplify the equations of motion for circularly polarized radiation, we can introduce a complex field

$$\hat{E} = \frac{E_\parallel - iE_\perp}{2}, \tag{1.17}$$

allowing these equations to be rewritten as

$$\dot{p} = -e\left[\hat{E}e^{i\overline{\theta}} + c.c\right] - \frac{p}{\tau} \tag{1.18}$$

and

$$\dot{\bar{\theta}} = \frac{\omega_L}{\gamma'} - \omega - \frac{e}{p}\left[i\left(\hat{E}e^{i\bar{\theta}} - c.c\right)\right]. \tag{1.19}$$

1.3 Electromagnetic field equations of motion and dynamics

The electromagnetic radiation field obeys the driven wave equation

$$-\nabla^2\mathbf{E} + \frac{1}{c^2}\frac{\partial^2\mathbf{E}}{\partial t^2} = -\mu_0\frac{\partial\mathbf{J}}{\partial t}. \tag{1.20}$$

Consider an electromagnetic wave of the form

$$\mathbf{E}_{(x,y,z,t)} = E_x\left(t - \frac{z}{c}, z\right)\hat{x} + E_y\left(t - \frac{z}{c}, z\right)\hat{y}, \tag{1.21}$$

which is propagating in the $+z$ direction. Making the substitution of variables

$$\bar{t} \equiv t - \frac{z}{c} \tag{1.22}$$

$$\partial/\partial t = \partial/\partial\bar{t} \tag{1.23}$$

$$\left(\frac{\partial}{\partial z}\right)_{old} = \left(\frac{\partial}{\partial z}\right)_{new} - \frac{1}{c}\frac{\partial}{\partial\bar{t}}. \tag{1.24}$$

The wave equation becomes

$$\left(\frac{1}{c^2}\frac{\partial^2}{\partial\bar{t}^2}\right)\left(E_{x(\bar{t},z)}\hat{x} + E_{y(\bar{t},z)}\hat{y}\right) - \left(\frac{1}{c}\frac{\partial}{\partial\bar{t}} - \frac{\partial}{\partial z}\right)^2\left(E_{x(\bar{t},z)}\hat{x} + E_{y(\bar{t},z)}\hat{y}\right) = -\mu_0\frac{\partial\mathbf{J}}{\partial t} = -\mu_0\frac{\partial\mathbf{J}}{\partial\bar{t}}, \tag{1.25}$$

or

$$\left(\frac{2}{c}\frac{\partial}{\partial\bar{t}}\frac{\partial}{\partial z}-\frac{\partial^2}{\partial z^2}\right)\left(E_{x(\bar{t},z)}\hat{x}+E_{y(\bar{t},z)}\hat{y}\right)=-\mu_0\frac{\partial\mathbf{J}}{\partial\bar{t}}. \tag{1.26}$$

Discarding the term $\partial^2/\partial z^2$ (negligible single-pass graphene reflection) and integrating with respect to $\bar{t}$ gives

$$\frac{2}{c}\frac{\partial}{\partial z}\left(E_{x(\bar{t},z)}\hat{x}+E_{y(\bar{t},z)}\hat{y}\right)=-\mu_0\mathbf{J}, \tag{1.27}$$

while omitting constant of integration since a nonvanishing zero-frequency component of radiation is unphysical. This result can in turn be integrated with respect to z, from just before radiation passes through the graphene to just after. The result is

$$\frac{2}{c}\Delta\left(E_{x(\bar{t},z)}\hat{x}+E_{y(\bar{t},z)}\hat{y}\right)=-\mu_0\int_{z\to0^-}^{z\to0^+}\mathbf{J}(z)dz, \tag{1.28}$$

where

$$\Delta\left(E_{x(\bar{t},z)}\hat{x}+E_{y(\bar{t},z)}\hat{y}\right)\equiv\left(E_{x(\bar{t},z)}\hat{x}+E_{y(\bar{t},z)}\hat{y}\right)\Big|_{z\to0^+}-\left(E_{x(\bar{t},z)}\hat{x}+E_{y(\bar{t},z)}\hat{y}\right)\Big|_{z\to0^-}. \tag{1.29}$$

Consider a charged quasi-fluid made of identical charged particles flowing at some velocity $\mathbf{v}=(v_x,v_y,v_z)$ through a box L_x by L_y by L_z (Fig. 1.3):

Let ρ be charge density, q be the charge of each charged particle, so that the number density of charges is ρ/q. The current going through the box in the $+x$ direction is

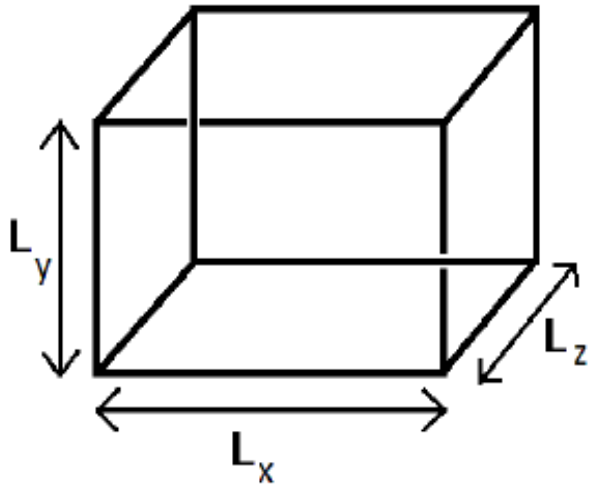

Fig. 1.3: Box representing a volume $L_x \times L_y \times L_z$.

$$I_x = \frac{\Delta Q_{YZ}}{\Delta t}, \tag{1.30}$$

where ΔQ_{YZ} is the charge flowing through $Y - Z$ face.

If charges have a velocity $\mathbf{v}$, the charges move in the x direction by $v_x \Delta t$ in time Δt, so charges in a volume $v_x \Delta t \times L_y \times L_z$ pass though the $Y - Z$ face in a time interval Δt. Hence

$$I_x = \frac{\rho v_x \Delta t L_y L_z}{\Delta t} = \rho v_x L_y L_z, \tag{1.31}$$

so

$$J_x = \frac{I_x}{L_y L_z} = \rho v_x. \tag{1.32}$$

A similar argument can be made for the other components, so $\mathbf{J} = \rho\mathbf{v}$.

If the velocity of charged particles is not uniform, simply replace $\mathbf{v}$ with its average over particles $\langle\mathbf{v}\rangle$, since each charged particle contributes independently to $\mathbf{J}$. Hence $\mathbf{J} = \rho\langle\mathbf{v}\rangle$ and

$$\int_{z\to 0^-}^{z\to 0^+} \mathbf{J}(z)dz = \left(\int_{z\to 0^-}^{z\to 0^+} \rho(z)dz\right)\langle\mathbf{v}\rangle = q\overline{n_0}\langle\mathbf{v}\rangle = -e\overline{n_0}\langle\mathbf{v}\rangle\,, \tag{1.33}$$

where $\overline{n_0}$ is the number of excited electrons per unit area. Using an earlier result (1.28) and the relation $Z_0 = \mu_0 c$, the relation (1.33) becomes

$$\Delta\left(E_{x(\bar{t},z)}\hat{x} + E_{y(\bar{t},z)}\hat{y}\right) = -\frac{Z_0}{2}\int_{z\to 0^-}^{z\to 0^+} \mathbf{J}(z)dz = \frac{eZ_0\overline{n_0}}{2}\langle\mathbf{v}(i,t)\rangle\,, \tag{1.34}$$

where Z_0 is the impedance of free space. Using Eq. (1.6) and simplifying notation, this becomes

$$\Delta\mathbf{E} = \frac{eZ_0\overline{n_0}}{2m'}\langle\mathbf{p}(i,t)/\gamma'(i,t)\rangle\,. \tag{1.35}$$

As will be explained in the Linear Theory, a more physical arrangement involves having forward and backward waves arriving at the graphene simultaneously, thus increasing the effective gain by a factor of 2. Incorporating this and expressing the result in terms of the complex field $\hat{E}$ from (1.17) gives the result

$$\Delta\hat{E} = \frac{eZ_0\overline{n_0}}{2m'}\left\langle\frac{p(i,t)e^{-i\bar{\theta}}}{\gamma'(i,t)}\right\rangle. \tag{1.36}$$

1.4 Necessity of electron inversion

There have been several papers in the quantum-mechanical literature that assume that gain occurs only when the electron population is inverted. This assumption should not be assumed to be unconditionally valid, because it is not so in the classical case. Only by assuming that there is no damping of the electron motion in the classical case does one recover that result. The following proof of this [T. Antonsen, personal communication] is included here to show that the existence of inversion-free lasing in the classical model with damping is an effect of including damping, not an unphysical result of treating the system classically.

In the absence of electron damping forces, the damping time $\tau \to \infty$. The rotating-frame electron equations (1.18) and (1.19) become

$$\dot{p} = -e\left[\hat{E}e^{i\bar{\theta}} + c.c\right], \tag{1.37}$$

and

$$\dot{\bar{\theta}} = \frac{\omega_L}{\gamma'} - \omega - \frac{e}{p}\left[i\left(\hat{E}e^{i\bar{\theta}} - c.c\right)\right]. \tag{1.38}$$

The electric field equation is still that from (1.36) (written now with subscripts suppressed and γ' being simply called γ),

$$\Delta\hat{E} = \frac{eZ_0\overline{n_0}}{2m'}\left\langle \frac{pe^{-i\bar{\theta}}}{\gamma} \right\rangle. \tag{1.39}$$

The momentum average can be expressed in terms of an electron distribution function $f(\overline{\theta}, p)$ as

$$\left\langle \frac{pe^{-i\overline{\theta}}}{\gamma} \right\rangle = \int_0^\infty \int_0^{2\pi} d\overline{\theta}\, dp\, p\ \frac{p}{\gamma} e^{-i\overline{\theta}} f(\overline{\theta}, p), \tag{1.40}$$

(since p is the Jacobian of the coordinate system) where f is a distribution function which is normalized so that

$$\int_0^\infty \int_0^{2\pi} d\overline{\theta}\, dp\ p[f(\overline{\theta}, p)] = 1. \tag{1.41}$$

Because electrons are neither created nor destroyed, the polar coordinate kinetic equation validly applies:

$$\frac{\partial f}{\partial t} + \frac{\partial}{\partial \overline{\theta}}(\dot{\overline{\theta}} f) + \frac{1}{p}\frac{\partial}{\partial p}(p\dot{p} f) = 0. \tag{1.42}$$

To write down a linear theory, let $f = f_0 + f_1$, where f_0 is a field-free term and f_1 is first order in $\hat{E}$. Because there is no damping and no field for f_0, the values of p are constants of the motion for it. Thus the kinetic equation for it is simply

$$\frac{\partial f_0}{\partial t} + \frac{\partial}{\partial \overline{\theta}} \dot{\overline{\theta}} f_0 = 0. \tag{1.43}$$

The solution is independent of angle (isotropic): $f_0 = f_0(p)$. The equation for the first order term is

$$\frac{\partial f_1}{\partial t} + \left(\frac{\omega_{_L}}{\gamma} - \omega\right)\frac{\partial f_1}{\partial \overline{\theta}} + (-e)[\hat{E}e^{i\overline{\theta}} + c.c.]\frac{\partial f_0}{\partial p} + \frac{1}{p}\dot{p}\, f_0 = 0. \tag{1.44}$$

It is now useful to introduce a function $\hat{f}_1(p,t)$, which is independent of $\overline{\theta}$, such that $f_1 = \hat{f}_1 e^{i\overline{\theta}} + c.c.$. Now the expression (1.40) simplifies to

$$\left\langle \frac{pe^{-i\overline{\theta}}}{\gamma} \right\rangle = 2\pi \int_0^\infty dp \frac{p}{\gamma}\hat{f}_1. \tag{1.45}$$

Eq. (1.44) becomes

$$\frac{\partial \hat{f}_1}{\partial t} + \left(\frac{\omega_{_L}}{\gamma} - \omega\right) i\hat{f}_1 - e\hat{E}\frac{\partial f_0}{\partial p} - e\hat{E}\frac{f_0}{p} = 0. \tag{1.46}$$

This equation can be solved by introducing the Laplace transformed function

$$\hat{F}_1(p,s) \equiv \int_0^\infty \hat{f}_1(p,t)e^{-st}dt \tag{1.47}$$

so that

$$s\hat{F}_1 + i\left(\frac{\omega_{_L}}{\gamma} - \omega\right)\hat{F}_1 - \frac{e\hat{E}\left(\frac{\partial f_0}{\partial p} + \frac{f_0}{p}\right)}{s} = 0, \tag{1.48}$$

which has the solution

$$\hat{F}_1 = \frac{e\hat{E}/s}{i\left[\frac{\omega_{_L}}{\gamma} - (\omega + is)\right]}\left(\frac{\partial f_0}{\partial p} + \frac{f_0}{p}\right). \tag{1.49}$$

Consider that due to the basic properties of Laplace transforms, in the limit $s \to 0^+$, $s\hat{F}_1 \to \hat{f}_1$. Thus,

$$\hat{f}_1 = \frac{e\hat{E}}{i\left[\frac{\omega_L}{\gamma} - (\omega + is)\right]}\left(\frac{\partial f_0}{\partial p} + \frac{f_0}{p}\right). \tag{1.50}$$

From (1.45), (1.39) and (1.50),

$$\Delta\hat{E} = \frac{e^2 Z_0 \overline{n_0}}{2m'}\, 2\pi \int_0^\infty dp \frac{p}{i\left[\omega_L - \gamma(\omega + is)\right]}\left(\frac{\partial f_0}{\partial p} + \frac{f_0}{p}\right)\hat{E}. \tag{1.51}$$

Gain may only occur when

$$G = Re\left[\int_0^\infty dp\, \frac{p}{i\left[\omega_L - \gamma(\omega + is)\right]}\left(\frac{\partial f_0}{\partial p} + \frac{f_0}{p}\right)\right] > 0. \tag{1.52}$$

Since

$$Re\left[\frac{1}{i(\omega_L - \gamma\omega) + \gamma s}\right] = \frac{\gamma s}{\gamma^2 s^2 + (\omega_L - \gamma\omega)^2}, \tag{1.53}$$

we find that if $(\partial f_0/\partial p + f_0/p) < 0$ for all p in the distribution, $G < 0$. Equivalently, gain cannot occur if

$$\frac{1}{p}\frac{\partial}{\partial p}(pf_0) < 0. \tag{1.54}$$

Since pf_0 is equivalent to the Cartesian coordinate momentum distribution function due to p being the Jacobian, this requirement implies that gain cannot occur when the distribution contains no inversion, in this case where $\tau \to \infty$.

A schematic of the device being considered is shown in Fig. (1.4).

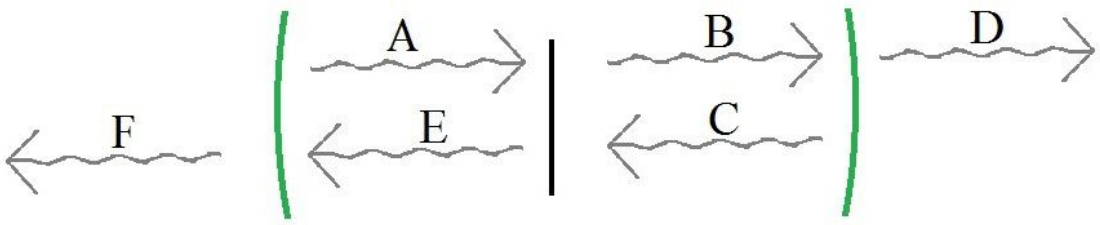

Fig. 1.4: Optically pumped graphene (black, pumping beam not shown) is sandwiched between two partially transmissive mirrors (green). In "forward wave only" mode, the beam is incident on the graphene (A). Beam then undergoes a gain due to the excited conduction electrons gyrating, and then undergoes an absorption by the graphene after this process (B). Beam is partially transmitted by a mirror (D) and partially reflected (C). Then the beam undergoes the same processes on the other side (E,F,A) and the cycle repeats itself. In "forward and backward wave" mode, half the THz energy is incident in the forward direction (A) while the other half is simultaneously incident on the graphene in the backward direction (C).

1.5 Chapters 2 and 3 overview

In Chapter 2, a linear model is developed, which allows a description of the dynamics of a THz oscillator when the electric field is weak. Under certain assumptions, a semi-analytical formula is derived, which shows that under some conditions,

an amplification of THz oscillation can occur which is sufficient to overcome losses of various types. This model is valid for predicting when the system will oscillate at all, but cannot predict how large the electric field will become, because once the field gets too strong, the linear model's assumptions are invalid.

Chapter 3 sets out to remedy this limitation. By numerically solving an alternate form of the equations of motion, the steady-state field strengths of the oscillator, and its output in steady state operation, are predicted.

Chapter 2: Linear Theory: Electron Cyclotron Resonance Gain in the Presence of Collisions

[The material in this chapter has been published in IEEE Transactions on Plasma Science. [20] Some material has been removed and transferred to the previous section of this thesis, and some trimmed material is added back in.

This chapter presents an analysis of the possibility of achieving gain for THz fields from a semiclassical perspective, and finds that it may be viable if the graphene is pumped by an external source, such as a mid-infrared laser of suitable strength, so that the graphene has an appropriate source of conduction electrons. We find gain even though there is no population inversion in the model. Gain is possible due to a correlation between an electron's energy and its time of birth. Previous work at low, zero, and negative Landau states such as in [8] concluded that Auger scattering prevents population inversion from occurring, and thus restricts gain. However the effect of Auger scattering at large quantum numbers is to contribute to an effective (classical) damping force. In the classical model, the Coulomb interaction between

electrons gives rise chiefly to small-momentum-transfer scattering events and can be thus approximated by a damping force on the electrons as they scatter by small angles and energy shifts from many other electrons successively. In the absence of a coherent radiation field, this slowing down also leads to a distribution function which decreases monotonically with increasing energy. However, if the slowing down and interaction with the radiation field are treated consistently we find gain is possible. While the full features of Auger scattering at low Landau levels require a quantum treatment, the classical treatment should suffice at large quantum numbers when many states are available for electrons to scatter into.

Electrons are pumped from the valence to the conduction band by the laser, so that the newly pumped electrons are in a narrow range of energies, but their momenta are isotropically distributed. When a monochromatic THz wave field is present, the electrons immediately are influenced by this field as they gyrate in the background magnetic field. The momenta, while initially isotropic, become anisotropic due to the interaction with the THz field. These electrons subsequently gyrate in the field, but the momentum distribution remains anisotropic. When the electrons lose energy due to dissipation, the gyration frequency increases (refer back to Eq. (1.1) for gyration frequency). For appropriately chosen THz field frequencies, the gyration frequency will, as it increases, briefly come into resonance with the THz field. Because of the anisotropic electron momentum distribution, there will be a net transfer of energy between the electrons and the field during the brief period in which the electrons are resonant with the THz field. Depending on the relative phase between the electrons and the field, this may result in the THz wave being

either amplified or attenuated. In this chapter, we explore the conditions required for the phases that result in amplification of the THz wave as it passes through the graphene.

While it may seem paradoxical that gain can occur without population inversion, one should bear in mind that the usual argument in the quantum-mechanical framework linking gain to population inversion assumes a *statistical* mixture (i.e. a completely *incoherent* superposition) of different energy levels. Indeed, the equivalent assumption in the classical picture (a gyroangle and time independent unperturbed distribution function) also results in a conclusion of no gain. Despite this, the phase bunching that occurs in the gyrating electrons can still give rise to gain when the electron birth times are correlated with their energies, as we will later show. This correlation leads to an energy-dependent gyration phase distribution relative to the phase of the THz field. Returning to the quantum mechanical picture, the assumption of statistically independent energy states does not apply to the case in our model, because a classical gyration phase, reinterpreted in quantum terms of a localized wave packet, is related to the relative phase between neighboring levels in a *coherent* superposition of energy eigenstates (Landau levels) with a common center of gyration. A bunching of classical gyration phases corresponds to the coherence within a quantum superposition of levels. Thus, the statistical/incoherent assumption usually invoked in atomic and molecular systems does not hold. A coherence between states has been shown to give rise to gain without inversion in systems with as few as three participating energy levels [21]. Thus the presence of a non-inverted population, is not by itself a sufficient condition to show that gain cannot occur.

Undoped graphene has the Dirac band structure [5], equivalent to ultrarelativistic (or massless) electrons, with a band velocity of 10^6 m/s. The conduction band and the valence band are touching at the Dirac point, as illustrated in Fig. 2.1a. The energy-momentum dispersion relation for the massless (zero band gap) band structure is

$$E = pc', \tag{2.1}$$

where c' is the band velocity. In the present study, we allow for the possibility of a band gap that could be achieved by doping and doubling the graphene to bilayer graphene [19], but the bandgap is not necessary and is taken to be small. The energy-momentum dispersion relation for the massive (nonzero band gap) band structure is

$$E = \sqrt{(pc')^2 + (m'c'^2)^2}, \tag{2.2}$$

where c' is the high-momentum band velocity and m' is the effective mass. The band gap energy is $2m'c'^2$. Furthermore, we assume that the Fermi level is tuned to $E = 0$, between the valence band and the conduction band. Thus, the electrons can be made to behave in a manner analogous to relativistic electrons in a conventional gyrotron. We also have the analogous relativistic factor γ' such that the energy is $E = \gamma' m' c'^2$ and the gyration frequency satisfies $\omega = eB/\gamma' m' = eBc'^2/E$.

The situation that we consider is illustrated in Fig. 2.1b. A sheet of graphene is oriented perpendicular to a uniform magnetic field. The graphene is illuminated

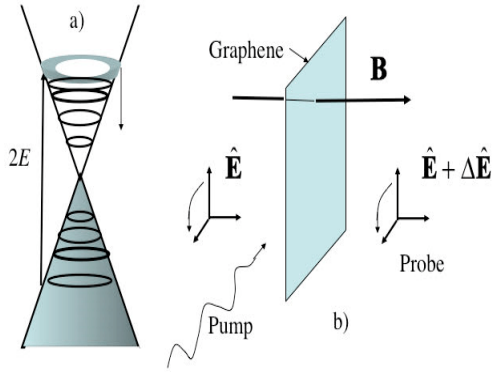

Fig. 2.1: a) Schematic of graphene band structure showing valence electrons and electrons excited by a laser pulse with photon energy $2E$. b) Schematic of configuration analyzed showing orientation of graphene sheet, applied magnetic field, and incident and transmitted probe wave. © 2017 IEEE.

by a pump and a probe. The pump beam excites an electron from the valence band to the conduction band as illustrated in Fig. 2.1a. The electron loses energy to collisions passing through multiple states of the ideal Hamiltonian while interacting with the wave electric field. The probe beam passes normally through the graphene and experiences gain or loss due to the response of the graphene electrons. Both the THz wave and the pump laser are assumed to have circular polarization so that the initial electron momentum distribution and the underlying dynamics are isotropic.

An exploration based on a classical treatment of electron motion in a strong applied magnetic field will be considered here and is valid when electron excitation energy is sufficiently large, such that the electrons responsible for the gain are in high

order Landau levels, with index $N \simeq [E^2 - (m'c'^2)^2]/(2\hbar|qB|c'^2) \gg 1$, where $\hbar$ is the reduced Planck constant. If we work in the low-band-gap limit where $E \gg m'c'^2$, this may be written as

$$N \simeq 7.6 \times 10^2 \frac{(E[\mathrm{eV}])^2}{(B[\mathrm{T}])}. \tag{2.3}$$

The gyration frequency of an electron with injected energy E_i is given by $\omega_i = eBc'^2/E_i$ with $c' = 10^6$m/s. Our analysis assumes that the electrons slow down due to collisions and thus, their gyrofrequency changes with time. We will find that maximum gain of the probe occurs due to electrons that have slowed such that their gyration frequency is a factor of about 1.7 times their initial frequency. The maximum gain occurs for frequencies

$$f[\mathrm{THz}] = 0.27 \frac{\mathrm{B[T]}}{\mathrm{E[eV]}}. \tag{2.4}$$

From Eqs. (2.3) and (2.4), the level number, frequency and energy relate via

$$N = 2.1 \times 10^2 \frac{E[\mathrm{eV}]}{f[\mathrm{THz}]}. \tag{2.5}$$

Thus for example, using an 8 T magnetic field as an upper limit, a 500 meV electron excited to the $N = 10^{th}$ state will give rise to gain at a frequency of 4 THz. The condition on N is more stringent than simply $N > 1$. This is because, as we will find, gain occurs in narrow bands of frequency $\delta f/f$ of order 0.2. It is necessary that there be a sufficient number of transitions in this frequency range so that the

classical picture involving a superposition of states can apply. Thus, we can expect to have to consider cases where N is of order 10 or higher.

To treat the situation we consider quantum mechanically one would need to include the effect of many transitions between states. Recall that the electron energy drops from its initial value to one that is roughly 50 % lower during the process of slowing down. Further, as we will find from the classical picture, the electron-field interaction occurs for a finite time, several wave periods. The quantum wave function describing this would thus involve a coherent superposition of multiple states. The classical approach accounts for these two effects in the limit of a large number of participating states, and provides an answer in terms of simple integrals and figures.

The organization of this chapter is as follows: In section II we derive classical equations for the gain or loss an electromagnetic wave experiences in crossing transversely a layer of graphene in which electrons have been energized. The main result of this analysis is an expression (Eqs.(2.35-2.39)) for the complex gain of the probe wave. This expression is evaluated numerically and the gain is plotted as a function of its independent parameters. The main conclusion is that positive gain can occur if the slowing down time τ satisfies $\omega_i\tau>15$. Section III presents a discussion of issues that are important in realizing gain experimentally and presents sample numbers. Finally, areas for further study are listed.

2.1 THz gain

We consider a single atomic layer of graphene that is illuminated by a mid-infrared laser to pump electrons from the valence band to the conduction band, at an initial energy $E_i = \sqrt{(p_i c')^2 + (m'c'^2)^2}$, corresponding to momentum p_i (Figure 2.1). A THz wave, to be amplified, is normally incident on the graphene. The electric field of this wave is in the plane of the graphene, $(x - y)$. The applied static magnetic field is perpendicular to the graphene plane (z). As long as the waist diameter of the THz beam is much larger than both the wavelength of the THz radiation and the distances (fast gyration and slow drift, if any) travelled by the electrons during their interaction with the radiation, the system is to a good approximation translationally invariant in both the x and y directions and will be treated as such in this analysis. The electrons are assumed to be governed by classical mechanics once injected into the conduction band by the IR laser.

The THz electromagnetic radiation field can be considered to undergo two processes in passing through the graphene. First, a modification by the current of the excited electrons in the graphene gives gain. Then, the field undergoes a dispersionless, frequency-independent loss due to absorption by the graphene itself. Mirror transmission, and mirror absorption (including large-angle scattering out of the cavity) would occur in a self sustaining oscillator as will be discussed in sec. III.

An electron at time t has a momentum $\mathbf{p}(t)$ which may be expressed in Carte-

sian coordinates as

$$\mathbf{p}(t) = p(t)[\cos\theta(t)\hat{x} + \sin\theta(t)\hat{y}]. \tag{2.6}$$

Differentiating the momentum with respect to time, using the damped Lorentz force relation with a collisional relaxation time τ gives $\dot{\mathbf{p}} = q\big[\mathbf{E} + \mathbf{v} \times \mathbf{B}\big] - \mathbf{p}/\tau$, and introducing the angle $\overline{\theta} = \theta - \omega t$, we obtain the pair of equations

$$\dot{p} = -e\left[\hat{E}e^{i\overline{\theta}} + c.c.\right] - \frac{p}{\tau}, \tag{2.7}$$

and

$$\dot{\overline{\theta}} = \frac{\omega_{_L}}{\gamma'} - \omega - ep^{-1}\left[i\hat{E}e^{i\overline{\theta}} + c.c.\right], \tag{2.8}$$

where

$$\omega_{_L} \equiv \frac{eB}{m'}, \tag{2.9}$$

$$\gamma' \equiv \sqrt{1 + \left(\frac{p}{m'c'}\right)^2}, \tag{2.10}$$

and

$$\hat{E} = \frac{(E_x - iE_y)}{2}e^{i\omega t}. \tag{2.11}$$

Our simple model treats inelastic scattering events of primarily small, longitudinal momentum transfers as an overall damping on the electron momentum causing

it to decay exponentially with time constant τ. Thus, we are excluding pitch angle and energy diffusion processes, with the rationale being that for superthermal electrons, damping should dominate. We note that in the absence of a coherent THz field the momentum relaxation term in Eq. (2.7) leads to a distribution function that scales with momentum as τ/p^2, and is thus not inverted.

We will solve this equation system subject to the following initial conditions. Electrons are injected into the conduction band with energy $E_i = \gamma_i m' c'^2$ with $\gamma_i = \left(1 + p_i^2/\left(m'c'\right)^2\right)^{1/2}$ and with initial momentum angle $\overline{\theta}$ uniformly distributed in the interval $[0, 2\pi]$. Further, each electron has a birth time t_B at which $p = p_i$ and $\overline{\theta} = \overline{\theta}_0$, which we will take to be uniformly distributed. Solutions are then parameterized as follows,

$$\begin{aligned} p &= p(t; \overline{\theta}_0, t_B) \\ \overline{\theta} &= \overline{\theta}_0 + \Delta\overline{\theta}(t; \overline{\theta}_0, t_B), \end{aligned} \tag{2.12}$$

where $p(t_B; \overline{\theta}_0, t_B) = p_i$, $\Delta\overline{\theta}(t_B; \overline{\theta}_0, t_B) = 0$.

We assume the radiation waist is sufficiently large so that we may take $\nabla \cdot \mathbf{J} \simeq 0$, and hence $\nabla \cdot \mathbf{E} \simeq 0$, and we consider the propagation of the electromagnetic fields to be essentially one-dimensional, in the z-direction, perpendicular to the plane of the graphene.

We combine the components of the wave equation for the electric field by projecting onto the basis function $(\hat{x} - i\hat{y})e^{i\omega t}/2$ and averaging over time to obtain

$$\frac{d^2}{dz^2}\hat{E}(z) + k^2\hat{E}(z) = -\frac{i\omega\mu_0}{2}\left\langle (J_x - iJ_y)e^{i\omega t}\right\rangle, \tag{2.13}$$

where $\mathbf{J} = \hat{x}J_x + \hat{y}J_y$ is the current produced by the graphene conduction electrons, $k = \omega/c$, and the angular brackets indicate the time average. We solve (2.13) using the method of variation of parameters. Specifically we write the electric field as the sum of a forward and backward wave,

$$\hat{E}(z) = \hat{E}_f(z)e^{ikz} + \hat{E}_b(z)e^{-ikz}, \tag{2.14}$$

where we constrain E_f and E_b by insisting $\partial\hat{E}_f/\partial z - \partial\hat{E}_b/\partial z = 0$. (We have replaced one variable, $\hat{E}$, by two, $\hat{E}_{f,b}$. Thus, we are free to make one relation relating $\hat{E}_f$ and $\hat{E}_b$.) Inserting the electric field (2.14) in the wave equation (2.13), using the constraint, and integrating the forward and backward waves through the graphene layer gives

$$\hat{E}_f(0+\epsilon) = \hat{E}_f(0-\epsilon) + \Delta\hat{E}_f \tag{2.15}$$

$$\hat{E}_b(0-\epsilon) = \hat{E}_b(0+\epsilon) - \Delta\hat{E}_b, \tag{2.16}$$

where

$$\Delta\hat{E}_f = \Delta\hat{E}_b = \frac{-c\mu_0}{4}\int_{z\to 0^-}^{z\to 0^+} dz \left\langle (J_x - iJ_y)e^{i\omega t}\right\rangle. \tag{2.17}$$

We assume the graphene is positioned halfway between the two mirrors such that when the forward and backward waves return to the graphene, they add coherently. Then on each transit, from graphene to mirror and back the field $\hat{E}(z=0)$ will increment by $\Delta\hat{E} = \Delta\hat{E}_f + \Delta\hat{E}_b$.

We now relate the current density in the graphene to the particle momentum in Eqs. (2.7) and (2.8).

Each conduction electron with velocity $\mathbf{v}(t;t_B,\overline{\theta_0}) = \mathbf{p}(t;t_B,\overline{\theta_0})/(\gamma(t;t_B,\overline{\theta_0})m')$ and birth time $t_B < t$, will contribute to the current density. If the pumping IR laser excites electrons to the conduction band at a rate $\dot{n}$, where $\dot{n}$ has units $m^{-2}s^{-1}$, the electric field change can be thus cast in terms of the velocity of an electron given its history as

$$\Delta\hat{E} = \frac{eZ_0\dot{n}}{2}\int_{-\infty}^{t} dt_B \left\langle (v_x - iv_y)e^{i\omega t}\right\rangle_{\overline{\theta_0}}, \tag{2.18}$$

where $Z_0 = \sqrt{\mu_0/\epsilon_0}$ is the impedance of free space and we have used $c = 1/\sqrt{\mu_0\epsilon_0}$. This gives the jump in the electric field the wave experiences due to the conduction electrons. The change in the complex amplitude $\hat{E}$ defined by Eq. (2.17) can then be expressed

$$\Delta\hat{E} = \frac{eZ_0\dot{n}}{2}\int_{-\infty}^{t} dt_B \left\langle (v_x - iv_y)\, e^{i\omega t}\right\rangle = \frac{eZ_0\dot{n}}{2m'}\int_{-\infty}^{t} dt_B \left\langle \frac{pe^{-i\bar{\theta}}}{\gamma}\right\rangle_{\bar{\theta}_0}. \tag{2.19}$$

We now seek to calculate the conditions under which the growth of a wave with prescribed frequency ω due to the interaction with the excited graphene electrons can overcome the combined losses due to absorption in the graphene and mirrors and transmission through the mirrors. To this end we assume that the electric field is oscillating sinusoidally, and is sufficiently small that the equations of motion can be linearized. We write the electron momentum as the sum of the field free component, with subscript "0", and a first order in electric field perturbation with subscript "1",

$$p\left(t-t_B\right)=p_0\left(t-t_B\right)+p_1\left(t-t_B\right), \tag{2.20}$$

and

$$\Delta\overline{\theta}\left(t-t_B\right)=\Delta\overline{\theta}_0\left(t-t_B\right)+\Delta\overline{\theta}_1\left(t-t_B\right). \tag{2.21}$$

The field free solutions satisfy Eqs. (2.7) and (2.8) with $\hat{E}$ set to zero,

$$p_0\left(t-t_B\right)=p_i e^{-(t-t_B)/\tau}, \tag{2.22}$$

and

$$\Delta\overline{\theta}_0\left(t-t_B\right)=\int_{t_B}^{t}dt'\left(\frac{\omega_{_L}}{\gamma_0\left(t'\right)}-\omega\right)=\left(\omega_{_L}-\omega\right)\left(t-t_B\right)-\omega_{_L}\tau ln\left(\frac{\gamma_i+1}{\gamma_0\left(t\right)+1}\right), \tag{2.23}$$

and

$$\gamma_0\left(t-t_B\right)=\sqrt{1+\frac{p_0^2\left(t-t_B\right)}{m'^2c'^2}}, \tag{2.24}$$

is the relativistic factor of an electron as it slows down, and

$$\gamma_i=\gamma_0(t=t_B), \tag{2.25}$$

is the initial relativistic factor.

In the first order equations the electric field appears. If we take ω to be the angular frequency of the (radiation) field, the quantity $\hat{E}$ defined in (2.11) will have

a steady (DC) component and a component oscillating at 2ω. In first order these act independently, so we take $\hat{E}$ to be DC. The first order equations for electron motion are written

$$\frac{d}{dt}p_1 = -\frac{p_1}{\tau} - \left(e\hat{E}e^{i\bar{\theta}_0+i\Delta\bar{\theta}_0} + c.c.\right), \tag{2.26}$$

and

$$\frac{d\Delta\bar{\theta}_1}{dt} = -\frac{\omega_L}{\gamma_0^2}\frac{d\gamma_0}{dp_0}p_1 - \frac{e}{p_0}\left(i\hat{E}e^{i\bar{\theta}_0+i\Delta\bar{\theta}_0} + c.c.\right). \tag{2.27}$$

We note from Eqs. (2.26) and (2.27) that the dependence of the momentum variables p_1 and $\Delta\bar{\theta}_1$ on the birth phase $\bar{\theta}_0$ can be separated according to $p_1 = \hat{p}_1(t-t_B)e^{i\bar{\theta}_0} + c.c.$ and $\bar{\theta}_1 = \Delta\hat{\bar{\theta}}_1(t-t_B)e^{i\bar{\theta}_0} + c.c.$. The complex amplitudes $\hat{p}_1$ and $\Delta\hat{\bar{\theta}}_1$ then satisfy

$$\frac{d\hat{p}_1}{dt} = -\frac{\hat{p}_1}{\tau} - e\hat{E}e^{i\Delta\bar{\theta}_0(t-t_B)}, \tag{2.28}$$

and

$$\frac{d\Delta\hat{\bar{\theta}}_1}{dt} = -\frac{\omega_L}{\gamma_0^2}\frac{d\gamma_0}{dp_0}\hat{p}_1 - i\frac{e}{p_0}\hat{E}e^{i\Delta\bar{\theta}_0(t-t_B)}, \tag{2.29}$$

with the initial conditions $\hat{p}_1(t=t_B) = \hat{\bar{\theta}}_1(t=t_B) = 0$.

Equations (2.28) and (2.29) can be integrated giving

$$\hat{p}_1 = -e\hat{E}\tau_A(t-t_B), \tag{2.30}$$

where

$$\tau_A(t) = e^{-t/\tau} \int_0^t dt' e^{t'/\tau + i\Delta\bar{\theta}_0(t')}, \tag{2.31}$$

and

$$\Delta\hat{\bar{\theta}}_1(t - t_B) = e\hat{E}\left[\int_{t_B}^t dt' \left(\frac{\omega_L}{\gamma_0^2}\frac{d\gamma_0}{dp_0}\tau_A(t' - t_B)\right) - \frac{i}{p_i}\tau_A(t - t_B)\right] \tag{2.32}$$

Next we linearize Eq. (2.19), which gives

$$\Delta E = \frac{eZ_0\dot{n}}{2m'}\int_{-\infty}^t dt_B \left(\left(\frac{1}{\gamma_0} - \frac{p_0}{\gamma_0^2}\frac{d\gamma_0}{dp_0}\right)\hat{p}_1 - i\frac{p_0}{\gamma_0}\Delta\hat{\bar{\theta}}_1\right) e^{-i\Delta\bar{\theta}_0}. \tag{2.33}$$

Upon substituting Eq. (2.30) and (2.32) in (2.33) and letting $\hat{t} = t - t_B$ such that $dt_B = -d\hat{t}$ we find for the increment in field amplitude

$$\Delta E = -\frac{e^2 Z_0\dot{n}}{4m'}\hat{E}\left(\int_0^\infty d\hat{t} e^{-i\Delta\bar{\theta}_0(\hat{t})}\left(\left(\frac{1}{\gamma_0^3(\hat{t})} + \frac{e^{-\hat{t}/\tau}}{\gamma_0(\hat{t})}\right)\tau_A(\hat{t})\right.\right. \tag{2.34}$$

$$\left.\left. + i\frac{p_0}{\gamma_0}\int_0^{\hat{t}} dt' \left(\frac{\omega_L}{\gamma_0^2}\frac{d\gamma_0}{dp_0}\right)\tau_A(t')\right)\right), \tag{2.35}$$

or simply

$$\frac{\Delta\hat{E}}{\hat{E}} = R\,(G - L)\,, \tag{2.36}$$

where

$$R = \frac{e^2 Z_0\dot{n}\tau^2 c'^2}{2E_i}, \tag{2.37}$$

is the dimensionless pumping rate, and

$$L = \gamma_i \int_0^\infty \left(\frac{1}{\gamma_0^3} + \frac{e^{-\hat{t}/\tau}}{\gamma_0} \right) \frac{\tau_A(\hat{t}) e^{-i\Delta\bar{\theta}_0(\hat{t})}}{\tau^2} d\hat{t}, \tag{2.38}$$

is a loss term representing absorption of THz by the energetic electrons,

$$G = -\gamma_i \int_0^\infty \frac{ip_0}{\tau^2 \gamma_0} \int_0^{\hat{t}} dt' \left(\frac{\omega_L}{\gamma_0^2} \frac{d\gamma_0}{dp_0} \right) \tau_A(t') e^{-i\Delta\bar{\theta}_0(\hat{t})} d\hat{t}, \tag{2.39}$$

is a potential gain term due to gyrophase bunching that allows the THz fields to be amplified. The real part of Eq. (2.36) describes the change in the magnitude of the electric field, while the imaginary part describes the change in phase.

Equation (2.36) describes the gain or loss the wave experiences on transmission through the graphene. Spontaneous oscillations can grow only for frequencies for which $g \equiv Re(G - L) > 0$, and physical gain of the entire system requires that the pumping rate $\dot{n}$ must be made large enough to overcome transmission, absorption, and scattering losses at the cavity's mirrors and the intrinsic absorption of energy by the valence band electrons of the graphene itself. The precise conditions leading to system gain ($Rg > \ell$, where ℓ represents all losses) will be addressed in the discussion section. For now, we will focus only on the conditions under which $g > 0$. The terms "gain" and "dimensionless gain" in this section, when not otherwise specified, will refer to $g = Re(G - L)$.

The functions G and L have been defined so that they are dimensionless by normalizing to the slowing down time squared. Since G has an extra time integration, we expect it to be larger than L when $\omega_i \tau \gg 1$. To further characterize the gain

we introduce the following parameters: the initial gyration frequency normalized by the slowing down time,

$$\omega_i \tau = \omega_{_L} \tau / \gamma_i = \frac{\tau[\text{ps}]\text{B}[\text{T}]}{E[\text{eV}]}, \tag{2.40}$$

the half bandgap energy normalized to the initial energy

$$m' c'^2 / E_i = \gamma_i^{-1}, \tag{2.41}$$

and the frequency normalized to the initial gyration frequency,

$$\omega / \omega_i = \gamma_i \omega / \omega_{_L}. \tag{2.42}$$

Plots of the real part of the dimensionless gain function versus frequency for several slowing down times are shown in Fig. 2.2. The intuitive understanding of the behavior of the system is in the Appendix. The dependence of g on frequency can be characterized as having a slowly varying average part (which is negative) and a superimposed rapidly varying part, which leads to intervals of frequency where gain is positive. Also shown in Fig. 2.2 as symbols are the frequencies associated with transitions between adjacent Landau levels for two cases: one in which the electrons are initially excited to the fifth Landau level, and one in which they are excited to the tenth. The classical limit should apply if these symbols are dense enough so that their spacing can resolve the gain curve.

The origin of the intervals of positive gain is explained as follows. Electrons are injected with initial energy, E_i. As an electron slows down, its resonant frequency increases. This means the horizontal axis of Fig. 2.2 also corresponds to time since birth of the electrons contributing to gain or loss at that frequency. The gain will then show oscillations with frequency corresponding to numbers of integer wave periods since birth. This can be shown as follows. The dependence of gain or loss on frequency enters Eq. (2.36) through the phase $\Delta\bar{\theta}_0(t-t_B)$ defined in Eq. (2.23). This phase is a rapidly varying function of time on the scale $t'/\tau \sim 1$, except for the interval of time when $\omega_{_L}/\gamma(t-t_B) \simeq \omega$. Expanding the time dependence of the phase around its stationary time, we have (Subscript "R" refers to resonance)

$$\Delta\bar{\theta}_0\left(t'\right) \simeq \phi_R + \frac{1}{2}\dot{\Omega}\left(t'-t_R\right)^2, \tag{2.43}$$

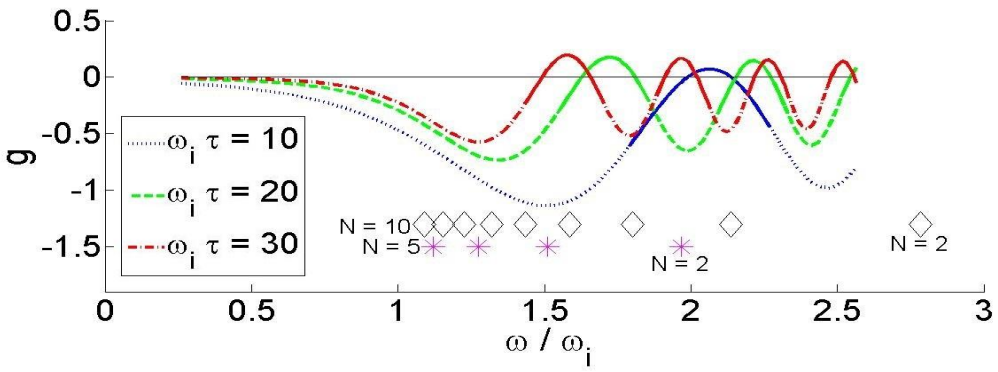

Fig. 2.2: Normalized gain versus normalized frequency for several dimensionless slowing down times. For this plot the normalized half bandgap energy is $m'c'^2/E_i = \gamma_i^{-1}$ = 0.00585. The solid portions of each curve indicate where $\cos(\phi_R + \pi/4) < 0$, where ϕ_R is defined in Eqs. (2.45) and (2.48). Diamonds and stars represent Landau transition energies for 3 T magnetic field, with the N = 10 (diamonds) and N = 5 cases (stars) arising at electron energies of 199 and 140 meV, respectively. g = Re(G-L) where G and L are defined by Eqs. (2.38) and (2.39), τ is the time scale of damping of electron motion, and the independent variables are explained by Eqs. (2.9), (2.40), (2.25), and (2.42). Amplification of the THz field cannot occur when g <0.

where t_R is defined by $d\Delta\bar{\theta}_0/dt' = 0$,

$$\frac{\omega_{_L}}{\gamma_0\left(t_R\right)}-\omega=0, \tag{2.44}$$

with

$$\phi_R=\int_{t_B}^{t_R}dt'\left(\frac{\omega_{_L}}{\gamma_0\left(t'\right)}-\omega\right), \tag{2.45}$$

and

$$\dot{\Omega}=\frac{d}{dt'}\frac{\omega_{_L}}{\gamma_0\left(t'\right)}\Big|_{t_R}=\frac{p_0^2\omega_{_L}}{\tau\gamma_0^3\left(m'c'\right)^2}\Big|_{t_R}. \tag{2.46}$$

The smooth part of the gain versus frequency curve comes from the contributions to the integrals in Eq. (2.39) from $\tau\simeq t_R$ with the additional approximation that the lower limit of the time integrals in Eqs. (2.31) and (2.35) is taken to be $\tau\to-\infty$. The rapid oscillations are due to the fact that the endpoint is in fact $\tau=0$, not $\tau\to-\infty$. These oscillations thus track the resonant phase ϕ_R defined in Eq. (2.45). The integral in (2.45) can be evaluated by switching from t' as the integration variable to $\gamma_0(t-t')$ defined through (2.24). The result is an expression for the resonant phase as a function of frequency,

$$\phi_R\left(\omega/\omega_{_L}\right)=\frac{\omega_{_L}\tau}{2} \tag{2.47}$$

$$\times\left\{\ln\left[\left(\frac{\gamma_i-1}{\gamma_i+1}\right)\left(\frac{\omega_{_L}/\omega+1}{\omega_{_L}/\omega-1}\right)\right]-\frac{\omega}{\omega_{_L}}\ln\left[\frac{\gamma_i^2-1}{(\omega_{_L}/\omega)^2-1}\right]\right\}. \tag{2.48}$$

The quantity ϕ_R corresponds to 2π times the number of wave periods that elapse between the birth of an electron at γ_i and the time it slows down to $\gamma_0=\omega_{_L}/\omega$.

To illustrate its importance we have modified the curves in Fig. 2.2 such that the curves are solid if $\cos(\phi_R + \pi/4) < 0$ and dashed if $\cos(\phi_R + \pi/4) > 0$. As can be seen, positive gain occurs only on solid portions of each curve. The origin of the $\pi/4$ phase shift, as well as a more rigorous explanation of the dependence of gain on resonance phase, is presented in the Appendix.

The effect of varying normalized half bandgap energy is shown in Fig. 2.3 where normalized gain is plotted vs. normalized frequency for three values of bandgap energy and fixed normalized slowing down time $\omega_i\tau = 44.1$.

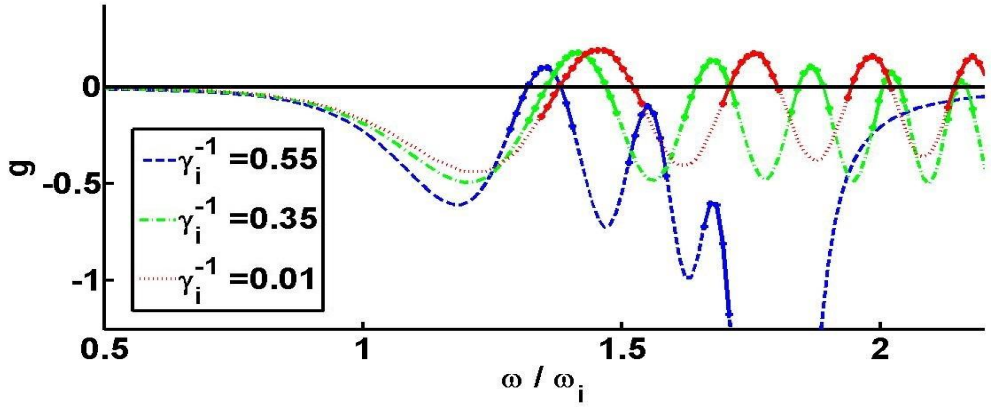

Fig. 2.3: Normalized gain versus normalized frequency (same variables as in Fig. 2.2) for several values of normalized half band gap energy. The normalized slowing down time is $\omega_i\tau = 44.1$ for all curves shown. The curves represent 3 selected half-band-gap energies γ_i^{-1} (see Eq. (2.41)). The solid portions of each curve indicate where $cos(\phi_R + \pi/4) < 0$, where ϕ_R is defined in Eqs. (2.45) and (2.48).

We see from Fig. 2.3 that the first gain peak is insensitive to the normalized half bandgap energy once γ_i^{-1} is small. Dips in gain occur at frequencies corresponding to the cyclotron resonance at the half bandgap energy $\omega/\omega_i = \gamma_i$. When electrons decrease their energy to the half bandgap value the gyration frequency becomes energy independent, and the negative mass effect responsible for cyclotron resonance gain no longer is possible.

The gain curves of the type shown in Fig. 2.2 and 2.3 have a series of local maxima as functions of ω/ω_i. We record for each pair of parameters γ_i^{-1} and $\omega_i\tau$ the maximum value of gain and plot these maxima as functions of $\omega_i\tau$ in Fig. 2.4.

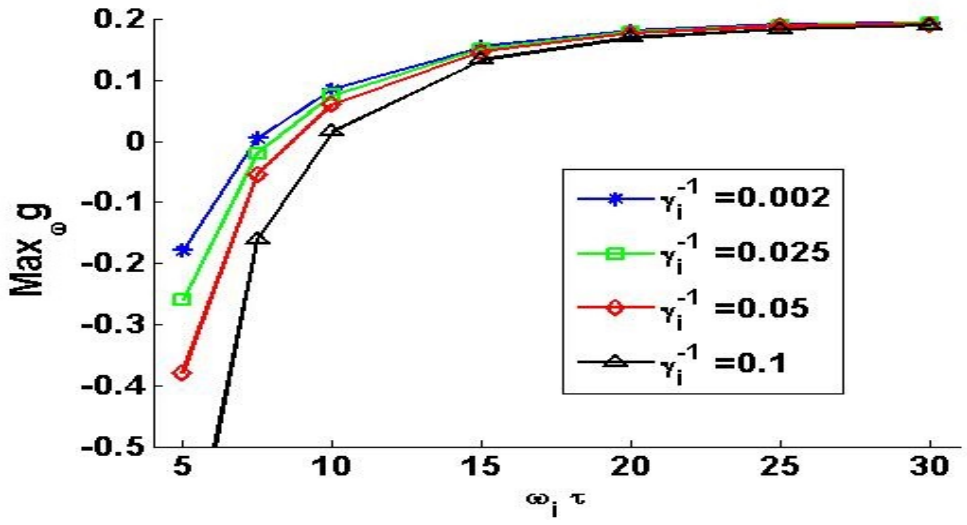

Fig. 2.4: Gain maximized over frequency as a function of slowing down time $\omega_i\tau$ and initial normalized half-bandgap γ_i^{-1}. © 2017 IEEE.

Two things are apparent in Fig. 2.4. First, the maximum in gain is relatively insensitive to the half bandgap energy once it is less than $\gamma_i^{-1} \leq 0.1$, and insensitive to slowing down time once it reaches $\omega_i\tau > 20$. We also notice that a slowing down time $\omega_i\tau > 15$ is required for sufficient gain. Figure 2.5 shows the frequency corresponding to the maximum gain points of Fig. 2.4 . We see that for $\omega_i\tau = 20$ the maximum gain occurs for a frequency $\omega/\omega_i \simeq 1.7$. The results of Figs. 2.4 and 2.5 will be used in the next section to determine the optimum dimensional parameters for observing gain.

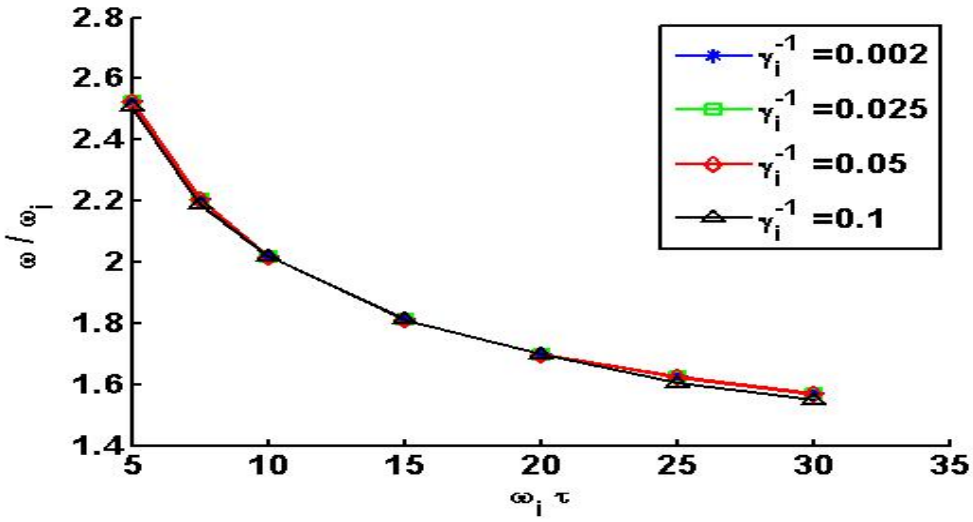

Fig. 2.5: Dimensionless frequency at which the gain peaks in Fig. (2.3) and (2.4) occur.

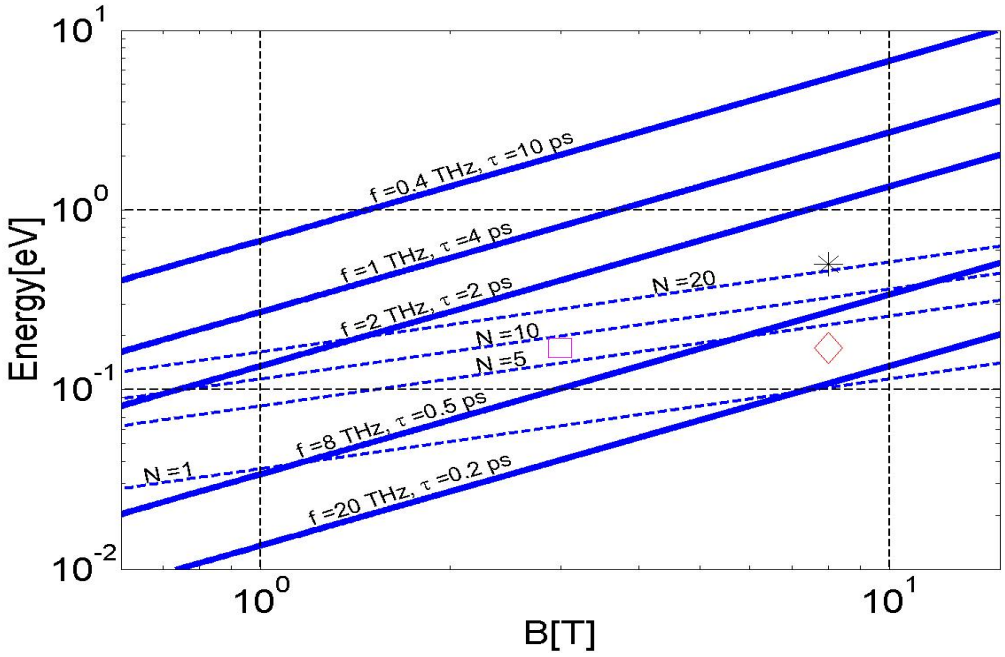

Fig. 2.6: Frequency and quantum index as a function of energy and magnetic field (log-log). Magenta square is 3 T magnetic field and 171 meV energy, the other two are 8 T field and 171 meV/500 meV (respectively). © 2017 IEEE.

2.2 Discussion

If THz gain is to be observed in experiments, or if a device producing THz radiation is to be constructed, parameters must be found such that the amplification of the THz field as expressed in Eq. (2.36) is sufficient to overcome the intrinsic losses. These are usually in the range of a few percent. In the case of the whole oscillator, the amplification would have to exceed, in addition, the losses and output coupling associated with the oscillator cavity.

The amplification expressed in Eq. (2.36) is the product of two factors: The

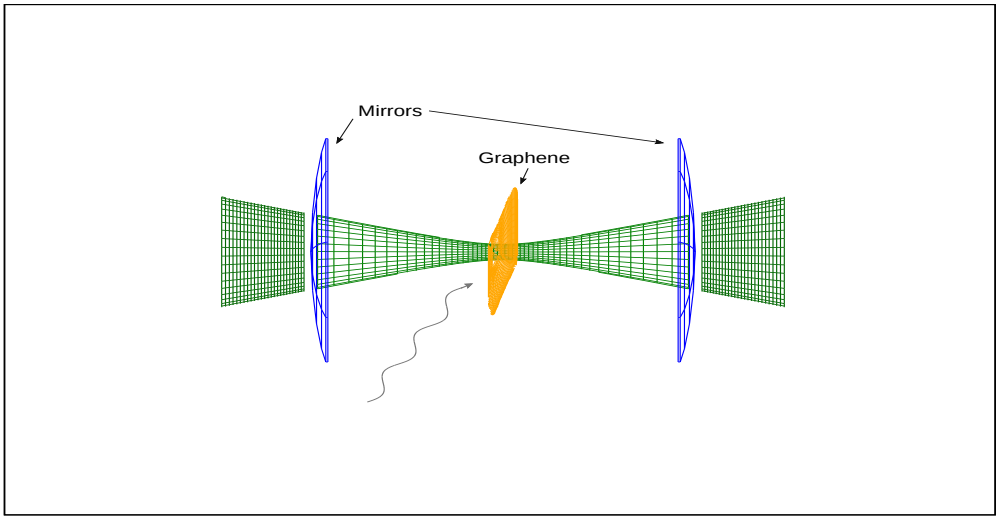

Fig. 2.7: Schematic of apparatus using mid-IR laser pumping. Partially transmissive curved mirrors (blue) form a cavity and contain a beam of THz radiation (green). This is amplified by the graphene (yellow-orange) which is pumped by mid-infrared radiation (gray wavy line) from a laser (not shown). The cavity is symmetric and gives two identical output beams (slightly darker green).

dimensionless gain, $g = Re(G - L)$, and a dimensionless ionization rate R given by (2.37). To be sufficient to overcome all losses, we must have $Rg > \ell$ for amplitude losses ℓ . Thus, the dimensionless gain g must be considered along with total cavity losses of all types in order to come up with the minimum value of R needed for the cavity to oscillate. These losses include mirror transmission, mirror scattering and absorption, and valence electron absorption in graphene, assumed to be 2.3 % of power for a monatomic layer. As an example of cavity loss, a mirror transmission $T = 0.0125$, mirror absorption/scattering α of 0.01, and graphene absorption ξ of 0.023, combine to form a cavity single pass *power* loss of $1 - (1 - T - \alpha)(1 - \xi) =$

0.045, or 4.5 %. The *amplitude* loss ℓ for this example is $1 - \sqrt{(1-T-\alpha)(1-\xi)}$ = 0.0228, or 2.28 %. Note that the assumed graphene absorption of 2.3 % is the standard absorption for a single layer of graphene, although that value is considered in much of the relevant literature (e.g. [22]) to be accurate only at higher frequencies than the THz range, and thus, may be a poor approximation at said frequencies. Since the normalized gain will be at best $g \sim 0.15$, it follows from Eq. (2.36) that an (extremely large) cavity amplitude loss of 15% implies a rate which must be in the range $R \sim 1$. For the minimal (graphene only) loss, we must have $R > 0.077$. We can rewrite R as follows,

$$R = 5.76 \times 10^2 \frac{(\tau[\text{ps}])^2}{E[\text{eV}]\tau_{\text{I}}[\text{ps}]}, \tag{2.49}$$

where $\tau_I = n_o/\dot{n}$ is an average ionization time and n_0 is the surface density of valence electrons, $n_0 = 3.82 \times 10^{19} m^{-2}$. The requirement $R > 0.077$ then gives

$$\frac{1}{\tau_I[\text{ps}]} > 1.34 \times 10^{-4} \frac{E[\text{eV}]}{(\tau[\text{ps}])^2}. \tag{2.50}$$

The ionization time also determines the pumping laser power per unit area absorbed, given by

$$I = \frac{2n_0 E_i}{\tau_I} = 1.643 \times 10^5 \left(\frac{E[\text{eV}]}{\tau[\text{ps}]}\right)^2 [\text{W/cm}^2]. \tag{2.51}$$

We note that if the constraint $\omega_i \tau = 20$ is imposed then,

$$I[\mathrm{W/cm^2}] = 4.11 \times 10^2 (\mathrm{B[T]})^2. \tag{2.52}$$

Possible operating points are displayed on Fig. 2.6 in a plot of the magnetic field vs. electron energy plane. Recall that the electron energy will be half the photon energy of the pumping laser. Two sets of lines are displayed in this plot. The solid lines are lines of constant frequency as given by Eq. (2.4). The dashed lines are lines of constant N as given by Eq. (2.3). The present analysis applies only to points well above the $N = 1$ line. Using the results of Fig. 2.2, we estimate that N > 10 is required. The set of lines labeled with frequency values show the energy and magnetic field needed to produce gain at the indicated frequency. Here we have taken the operating frequency to be a factor 1.7 times greater than the initial gyration frequency such that it is given by Eq. (2.4). Operation at a specified frequency requires that the slowing down time be sufficiently long such that $\omega_i \tau \geq 20$. Thus, curves of constant operating frequency also correspond to curves of required slowing down time. As far as parameter choices are concerned, high electron energies make the mean free time too short, for example, at electron energies in the 0.5-1 eV range (asterisk in Fig. 2.6 is at 500 meV), the mean free time is only around 100 fs or less due to the hot electrons losing energy to interband transitions ("impact ionization") [23,24]. For this and other reasons, the parameter choices corresponding to Fig. 2.2 seem more reasonable and are shown by the diamond on Fig. 2.6. At this low energy (corresponding to an oscillator operation frequency of 12.6 THz if the magnetic field is 8 T), the energy loss rate should be small because 171 meV is below

the threshold for optical phonon emission [25]. Note also that magnetic fields can increase intraband relaxation times in graphene [26, 27]. The absorbed pump laser power required for this example follows from Eq. (2.52) and is $2.63 \times 10^4 \mathrm{W/cm}^2$. If this power is absorbed in an area whose diameter is 20 wavelengths at 12.63 THz, the required absorbed power is ~ 47 W. The square shows a reduced magnetic field that corresponds to a higher quantum level number, which can be considered to make sure the classical formulas are applicable.

Up until now we have only considered the single pass amplification of a THz wave incident on a single layer of graphene. If a self-sustaining oscillator is desired, it would be configured as shown in Fig. (2.7). The graphene would be placed between two mirrors that define a Fabry-Perot resonator, and the THz wave would pass repeatedly through the graphene. The THz signal would grow from noise, if the gain were sufficient to overcome losses, $Rg > \ell$ where ℓ represents the amplitude loss factor per half trip through the resonator. As mentioned, contributing to ℓ are the intrinsic losses in the graphene, losses in the mirrors, and any fractional losses due to output coupling.

Two important issues to be addressed in the classical picture are the determination of operating frequency and determination of the saturation level of THz radiation. If the frequency were known, determination of the saturation level could be made by returning to Eqs. (2.7) and (2.8) and solving them numerically with a prescribed field amplitude $\hat{E}$. The recorded trajectories $p(t-t_B, \theta_0)$ and $\theta(t-t_B, \theta_0)$ would then be inserted in Eq. (2.19) and a nonlinear gain would be computed. This calculation should be repeated for different amplitudes until the amplitude was found

for which the nonlinear gain balanced the losses.

The determination of the operating frequency will require a treatment of the competition between the different modes of the Fabry-Perot resonator. From Fig. 2.2 and Fig. 2.3 we see that the gain vs. frequency has a series of peaks. The fractional width of a single peak is about $\Delta f/f \simeq 0.1$. Thus, if the spacing between mirrors is L = 1 cm, the separation in frequency between adjacent modes is $\pi c/L =$ 90 GHz. Taking the operating frequency to be 12.6 THz and the gain bandwidth to be 1.26 THz implies that only fourteen modes could have gain. The competition among modes could then be treated via expansion of the field in modes with slowly evolving amplitudes.

Another issue worthy of deeper study is the effects of collisions on the electron motion. We have modeled the effect as a steady slowing down. The collision process may also involve scattering in pitch angle and energy. A simple estimate of the sensitivity of our results to the inclusion of these effects can be made by examining the dependence of gain on slowing down time in Fig. 2.2. We note that it requires a change in slowing down time from $\omega_i\tau = 20$ to $\omega_i\tau = 30$ to move the positive gain band of frequencies by an amount equal to its width. Thus, to the extent that the additional collision processes can be modeled as less than a 50% variation in slowing down time the conditions for gain are robust.

2.3 Conclusion

In conclusion, cyclotron resonance gain occurs at some frequencies if the electrons have a long enough slowing down time and are assumed to not undergo large-angle scattering. Results are promising and net gain in the THz frequency regime for an oscillator might be possible considering cavity, graphene absorption, and output coupling, but some questionable assumptions were made, particularly concerning which scattering processes of electrons in graphene can be neglected, and how to treat the others.

Of course, this analysis requires caution regarding the usage of classical physics, which is valid only when the electron kinetic energy is a large multiple of the gyration quantum energy, $N \gg 1$. The scattering time is now realistically in accordance with modern experimental values, as the scattering time is distinct from that of thermal electrons and is enhanced by the presence of a magnetic field. This magnetic field increases the carrier lifetime significantly above that which is otherwise observed and reported in the literature.

A more complete analysis would also look at possible quantum corrections, thermal excitation effects, and factor in the electron-hole cross section both for scattering and creation (per carbon atom) by the IR laser. More complex mirrors could also be considered.

2.4 Acknowledgements

We are pleased to acknowledge discussions with Ed Ott, Thomas Murphy , Martin Mittendorff, and Michael Fuhrer. This work was partially supported by the Naval Research Laboratory (N00173131G018) and the Office of Naval Research (N000140911190).

2.5 Appendix: Semi-analytical treatment of integrals

In this section, we aim to explain the behavior seen in Fig. 2.2 by making approximations to Equation (2.39) so as to make it possess a closed-form solution. Equation (2.39) with $\tau_A(t')$ expanded,

$$G = -\gamma_i \int_0^\infty d\hat{t} e^{-i\Delta\bar{\theta}_0(\hat{t})} \frac{ip_0}{\tau^2\gamma_0} \int_0^{\hat{t}} dt' \left(\frac{\omega_L}{\gamma_0^2}\frac{d\gamma_0}{dp_0}\right) e^{-t'/\tau} \times \int_0^{t'} dt'' e^{t''/\tau + i\Delta\bar{\theta}_0(t'')}, \tag{A1}$$

can be re-expressed with the lower endpoint contribution of the innermost integral made explicit:

$$G = \frac{G_2 - G_1}{\tau^2}, \tag{A2}$$

with

$$G_1 = \gamma_i \int_0^\infty d\hat{t} e^{-i\Delta\bar{\theta}_0(\hat{t})} \frac{ip_0}{\gamma_0} \int_0^{\hat{t}} dt' \left(\frac{\omega_L}{\gamma_0^2}\frac{d\gamma_0}{dp_0}\right) e^{-t'/\tau} \times \int_{-\infty}^{t'} dt'' e^{t''/\tau + i\Delta\bar{\theta}_0(t'')} \tag{A3}$$

$$G_2 = \gamma_i \int_0^\infty d\hat{t} e^{-i\Delta\bar{\theta}_0(\hat{t})} \frac{ip_0}{\gamma_0} \int_0^{\hat{t}} dt' \left(\frac{\omega_L}{\gamma_0^2} \frac{d\gamma_0}{dp_0} \right) e^{-t'/\tau} \times \int_{-\infty}^0 dt'' e^{t''/\tau + i\Delta\bar{\theta}_0(t'')}. \tag{A4}$$

It may now be noted that the innermost integral in G_2 is separable from the rest since the bounds of integration are fixed and thus the inner integral is independent of the dummy variables in the outer integrals and acts as a constant with respect to them:

$$G_2 = \left[\gamma_i \int_0^\infty d\hat{t} e^{-i\Delta\bar{\theta}_0(\hat{t})} \frac{ip_0}{\gamma_0} \int_0^{\hat{t}} dt' \left(\frac{\omega_L}{\gamma_0^2} \frac{d\gamma_0}{dp_0} \right) e^{-t'/\tau} \right] \times \left[\int_{-\infty}^0 dt'' e^{t''/\tau + i\Delta\bar{\theta}_0(t'')} \right]. \tag{A5}$$

Recall that $e^{-i\Delta\bar{\theta}_0(\hat{t})}$ is rapidly oscillatory except around $\hat{t} = t_R$, so the outermost integral in ((A5)) gets its main contribution from that time. For low frequencies such that $t_R << \tau$, we can thus approximately evaluate that integral by invoking $e^{-t'/\tau} \simeq 1$, $p_0(t') \simeq p_0(t) \simeq p_i$, and $\gamma_0(t') \simeq \gamma_0(t) \simeq \gamma_i$, so we have (using $d\gamma_0/dp_0 = p_0/((m'c')^2\gamma_0)$):

$$\gamma_i \int_0^\infty d\hat{t} e^{-i\Delta\bar{\theta}_0(\hat{t})} \frac{ip_0}{\gamma_0} \int_0^{\hat{t}} dt' \left(\frac{\omega_L}{\gamma_0^2} \frac{d\gamma_0}{dp_0} \right) e^{-t'/\tau} \tag{A6}$$

$$\simeq \gamma_i \int_0^\infty d\hat{t} e^{-i\Delta\bar{\theta}_0(\hat{t})} \times \frac{ip_i}{\gamma_i} \int_0^{t_R} dt' \left[\frac{\omega_L}{\gamma_i^2} \frac{p_i}{(m'c')^2\gamma_i} \right] \tag{A7}$$

$$= \gamma_i \int_0^\infty d\hat{t} e^{-i\Delta\bar{\theta}_0(\hat{t})} \frac{ip_i}{\gamma_i} (t_R) \left[\frac{\omega_L}{\gamma_i^2} \frac{p_i}{(m'c')^2\gamma_i} \right]. \tag{A8}$$

From (A8) and ((A5)),

$$G_2 \simeq -K_0 \int_0^\infty d\hat{t} e^{-i\Delta\bar{\theta}_0(\hat{t})}, \tag{A9}$$

where K_0 is an overall constant factor.

Now the integral in (A9) may be evaluated by noting that the complex exponential is rapidly oscillatory except around $\hat{t} = t_R$ so that it should not make a significant difference whether the lower limit of the integral is at $\hat{t} = 0$ or at $\hat{t} = -\infty$. Thus,

$$\int_0^\infty d\hat{t} e^{-i\Delta\bar{\theta}_0(\hat{t})} \simeq \int_{-\infty}^\infty d\hat{t} e^{-i\Delta\bar{\theta}_0(\hat{t})}. \tag{A10}$$

Now we note that the quadratic phase approximation (2.43) may be substituted into (A10), giving

$$\int_0^\infty d\hat{t} e^{-i\Delta\bar{\theta}_0(\hat{t})} \simeq \int_{-\infty}^\infty d\hat{t} e^{-i\phi_R} e^{-i\frac{\dot{\Omega}}{2}\left(\hat{t}-t_R\right)^2} \tag{A11}$$

$$= e^{-i\phi_R}\sqrt{\frac{2}{\dot{\Omega}}}\int_{-\infty}^\infty e^{-iu^2} du, \tag{A12}$$

where ϕ_R is defined by (2.45), and we have made the u-substitution $u = \left(\hat{t} - t_R\right)\sqrt{\dot{\Omega}/2}$. This may be evaluated using Fresnel integrals, giving

$$\int_0^\infty d\hat{t} e^{-i\Delta\bar{\theta}_0(\hat{t})} \simeq e^{-i\left(\phi_R + \frac{\pi}{4}\right)}\sqrt{\frac{2\pi}{\dot{\Omega}}}. \tag{A13}$$

This result (A13) can be inserted in (A9):

$$G_2 \simeq -K_0 e^{-i\left(\phi_R+\frac{\pi}{4}\right)}\sqrt{\frac{2\pi}{\dot{\Omega}}}. \tag{A14}$$

The gain, G may now be evaluated using (A2) with the approximation $G_1 << G_2$ and the result (A14):

$$G \simeq -K_1 e^{-i\left(\phi_R+\frac{\pi}{4}\right)}, \tag{A15}$$

with K_1 being a new overall constant which absorbs some other terms. Thus, $g>0$ is only expected to occur when $cos\,(\phi_R + \pi/4) <0$, in excellent agreement with the numerically integrated result displayed in Fig. 2.2. Note that this crude approximation works well when at frequencies near to, but slightly above, $\omega_{_L}/\gamma_i$. The value at lower frequencies is an unphysical artifact since t_R does not exist. At frequencies much above $\omega_{_L}/\gamma_i$, the approximation performs poorly due to the fact that the assumptions $p_0(t_R) \simeq p_i$ and $\gamma_0(t_R) \simeq \gamma_i$ no longer hold.

Chapter 3: Nonlinear Theory: Nonlinear Gyrotron-like THz source based on Graphene

[Material intended to be reused in whole or in part for a journal publication, preferably also in IEEE Transactions on Plasma Science.]

3.1 Introduction

Cyclotron radiation is produced when electrons gyrate in a magnetic field, and are consequently continually accelerating and radiating. The gyrotron produces radiation similar to cyclotron radiation, but makes use of the relativistic dependence of the gyration frequency on energy to create stimulated emission. Gyrotron radiation has been analyzed using both linear and nonlinear theories since at least 1960 [14]. In the non-relativistic case, the electron gyration frequency is independent of electron energy, which means that stimulated emission cannot occur. However, for relativistic electrons, the gyration frequency does have energy dependence, which the gyrotron exploits to amplify a radiation field. Depending on an electron's gyration phase relative to that of the EM field, the electron will be accelerated or decelerated. Those that are accelerated have a reduced gyration frequency, forming a nonuniform distribution in gyrophase, which reinforces the growth of the electric

field. Both classical and quantum descriptions of this have been found to predict this amplification [14].

Traditional cyclotrons and gyrotrons are limited by the electron mass to a (cyclical) frequency of 28 GHz/Tesla, assuming the main operation is at the fundamental frequency. Thus gyrotrons, while an excellent source of microwaves at frequencies up to hundreds of GHz, are not a suitable source for Terahertz radiation, unless an extremely strong magnetic field is used. Electrons in graphene have a much smaller effective mass than electrons *in vacuo*, thus circumventing this limitation. Note, however, that using graphene electrons as a gyrotron-like source has some limitations that electrons in a conventional gyrotron do not. In particular, electrons in graphene must be excited to the conduction band in order to be useful, and then these electrons may lose energy by a variety of dissipative scattering processes as well as gyrotron radiation. Among these processes are Auger scattering, electron-hole scattering, and others. These dissipative scattering mechanisms cause much of the device energy to be lost as heat. Despite this, the ability of these oscillators to operate at Terahertz frequencies, even with modest applied magnetic fields, makes them a potentially useful source of Terahertz radiation. This work aims to explore, using numerical calculation, the operation of a graphene-based terahertz oscillator.

A discussion of the early literature on solid-state analogs of cyclotron resonance masers can be found in [1]. Some of this work also included analyses of lasing

by holes, rather than, or in addition to, electrons. In the earlier literature and also more recently, a number of authors have proposed solid state sources of THz radiation based on electrons, including Landau-level lasing, which is the quantum description of the gyrotron process. [6] [7] [8] Unlike the most common approach used by previous authors, this analysis is conducted in the classical limit, when the quantum numbers of the Landau states involved are much larger than unity.

Holes gyrate in the opposite sense from electrons, due to their positive electrical charge. This is true in the same way that holes' curvature in a magnetic field in the classical Hall effect is opposite the curvature of electrons. Hence the gyrating holes do not appreciably couple to circularly polarized radiation of the same handedness that couples to electrons, when the geometry is such that the Terahertz wave propagation direction and the static magnetic field are both perpendicular to the plane of the graphene. In this work, holes are omitted from the analysis and only electrons are considered.

This work builds upon an earlier paper [20], in which it is predicted, using a linear model and classical dynamics for both the electrons and the field, that gain can occur in a graphene-based THz gyrotron oscillator under certain conditions. In optically pumped monolayer graphene which is in a low-loss cavity, conduction electrons may exhibit gyrotron-like behavior. In order for net amplification to occur, a sufficiently low rate of energy loss from the electrons is required. As in the previous paper, the energy loss of the electrons due to inelastic scattering is included by

adding a damping force to the electrons' equations of motion, as will be presented in the next section. In this work, the problem is approached numerically considering both single-frequency and multiple-frequency operation of the oscillator. A discussion of how the dynamics becomes nonlinear with increasing THz field strength is presented.

It should be noted that in reality, electromagnetic fields inside a cavity can have very complex spatial profiles which depend on the cavity geometry and on the particular cavity mode(s) which are excited in the oscillator. For simplicity, the model used here takes the radiation field to be homogeneous in the directions transverse to the radiation propagation, that is, it as though the field were that of a plane wave. The electric field is thus taken to be a function of only z and t, and it propagates through graphene which is in the x-y plane. Future research could improve upon this model by allowing the radiation field to have a more complex spatial form, for instance, a Laguerre-Gaussian. Additionally, this analysis assumes a static, homogeneous magnetic field imposed on the graphene in addition to the radiation field, and this field is taken to be in the z-direction.

One may question the assumption of a single slowing down time and the effect of having electrons that lose energy at varying rates. To test this, the gain curves can be plotted for varying slowing down times in the linear model, before embarking on the development of the nonlinear model which also assumes the validity of the assumption of a single slowing down time τ for all simulated electrons. This is shown in Fig. (3.1).

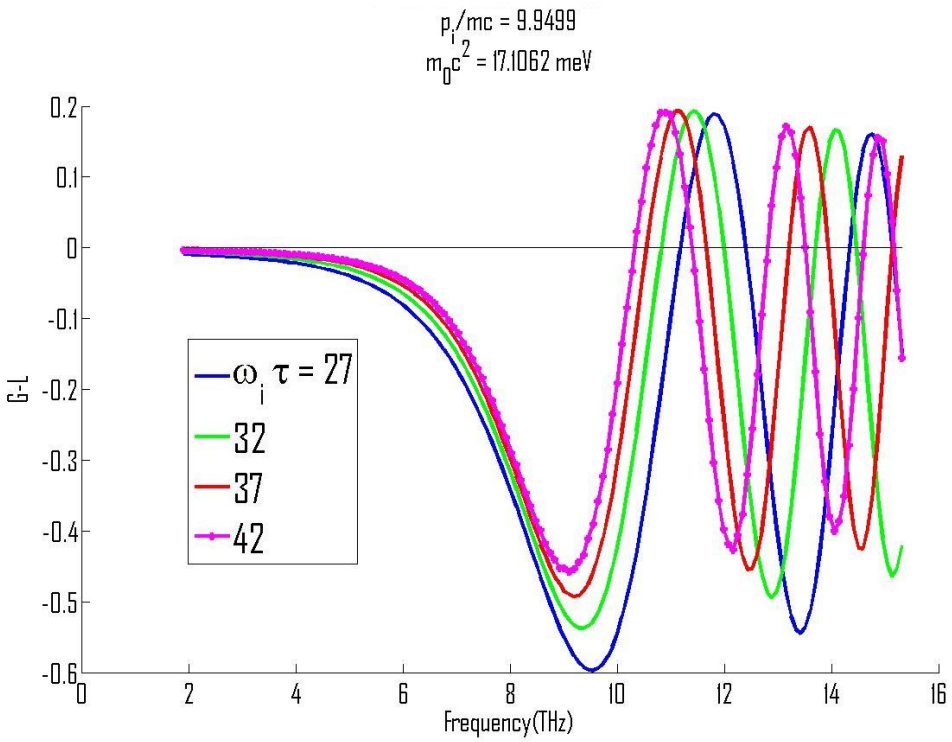

Fig. 3.1: Dynamics: different slowing down times superimposed with the same ω_i. Inelastic scattering which acts as a variation in the slowing-down time τ still can allow gain to occur in frequency ranges where the gain is positive across the range of τ values. Here is an example of how this could be the case. In a narrow range of frequences between 10 and 12 THz, all the gain curves are positive for $\omega_i\tau$ values running from 27 to 42.

The concurrence of gain for a range of slowing down times allows for a stochastically-varying energy loss rate in the electrons, and shows that it might not prevent gain from occurring in the system.

3.2 Theory

The classical frequency of gyration for a single electron in only a static magnetic field is given by $\omega = 2\pi\nu = eB/(\gamma m_e)$, where $\gamma = (1 - v^2/c^2)^{-1/2}$. This reduces to the cyclotron frequency relation $\omega = eB/m_e$ in the non-relativistic limit, giving rise to the fundamental limit of 28 GHz/Tesla mentioned earlier. Electrons in impure graphene, with a bandgap, have an energy-momentum relation of the form

$$E = \sqrt{(pc')^2 + (m'c'^2)^2}, \tag{3.1}$$

where c' is the high-momentum band velocity and m' is the effective mass [20]. (For graphene, the high momentum band velocity is very nearly 10^6 m/s.) This allows the graphene gyrotron to reach the higher frequencies in the Thz range.

The oscillator to be modeled is taken to be composed of two partially reflective mirrors with the optically pumped graphene sandwiched between the two mirrors. The two mirrors are taken to be identical, each having a power transmission coefficient T and power absorption coefficient α. The graphene has a power absorption coefficient ξ. All of these factors serve to remove power from the recycled beam on each half-round-trip of the THz radiation inside the cavity formed by the two mirrors. As in [20],ζ, the total cavity power loss per half-round-trip, is related to each loss via

$$\zeta = 1 - [(1 - T - \alpha)(1 - \xi)]. \tag{3.2}$$

.

As described in [20], an electron moving within the x-y graphene plane under the influence of a THz wave has a momentum that may be described in terms of its magnitude and direction as a function of time:

$$\mathbf{p}(t) = p(t)[\cos\theta(t)\hat{x} + \sin\theta(t)\hat{y}]. \tag{3.3}$$

The electron is considered to be "born" (pumped into the conduction band) at some time t_B and subsequently follows the equations of motion for this momentum, which may be found using the Lorentz force law and adding an electron damping force $\dot{p}_{damping} = -p/\tau$, giving

$$\dot{p}(t) = -e[E_x(t)\cos\theta(t) + E_y(t)\sin\theta(t)] - \frac{p(t)}{\tau}, \tag{3.4}$$

and

$$\dot{\theta}(t) = -p(t)^{-1}e[-E_x(t)\sin\theta(t) + E_y(t)\cos\theta(t)] + \frac{\omega_{_L}}{\gamma'(t)}, \tag{3.5}$$

where the last term represents the gyration of the electron in a static magnetic field B which is normal to the graphene plane, E_x and E_y are the Cartesian components of the THz wave's electric field,

$$\omega_{_L} \equiv \frac{eB}{m'}, \tag{3.6}$$

and

$$\gamma'(t) \equiv \sqrt{1 + \left(\frac{p(t)}{m'c'}\right)^2}, \tag{3.7}$$

where m' is the electron's effective mass and c' is the band velocity, approx. 10^6 m/s. (Note that these equations of motion for each electron are valid only for times $t > t_B$. In our model, we assume there are electrons born at differing times t_B, because the pumping is continuous.)

Now we assume a circularly polarized THz "seed" field which can be described by its complex amplitude (The subscript t will now be omitted for clarity/brevity):

$$\hat{E} = \frac{(E_x - iE_y)}{2} e^{i\omega t}. \tag{3.8}$$

This allows us to transform to a rotating frame at angular velocity ω and angle ϕ_0 (which we take to be uniformly distributed) by introducing the rotating frame angle $\overline{\theta} = \theta - \omega t - \phi_0$. The equations of motion may be written in terms of these new variables as

$$\dot{p} = -e\left[\hat{E}e^{i\overline{\theta}} + c.c.\right] - \frac{p}{\tau}, \tag{3.9}$$

and

$$\dot{\overline{\theta}} = \frac{\omega_L}{\gamma'} - \omega - ep^{-1}\left[i\hat{E}e^{i\overline{\theta}} + c.c.\right]. \tag{3.10}$$

Electrons following these equations of motion may gain energy from the field, or lose energy to the field. A self-consistent theory, of course, needs to account not only for the effect of the field on the electrons, but also the effect of the electrons on the field. Maxwell's equations allow us to relate the current, which is the collective

flow of charge, to the source of the electromagnetic field. The driven electromagnetic wave equation is

$$-\nabla^2\mathbf{E} + \frac{1}{c^2}\frac{\partial^2\mathbf{E}}{\partial t^2} = -\mu_0\frac{\partial\mathbf{J}}{\partial t}, \tag{3.11}$$

which allows radiation to be absorbed and emitted by matter containing some current density $\mathbf{J}$. For radiation travelling in the "+z" direction passing through graphene which is in the x-y plane, it is useful to define the change in radiation field [20]

$$\Delta(\mathbf{E}) \equiv (E_x(\bar{t},z)\hat{x} + E_y(\bar{t},z)\hat{y})\big|_{z\to 0^+} - (E_x(\bar{t},z)\hat{x} + E_y(\bar{t},z)\hat{y})\big|_{z\to 0^-}. \tag{3.12}$$

This may be evaluated using the driven wave equation by rewriting into integral form, giving [20]

$$\Delta\mathbf{E} = -\frac{c\mu_0}{2}\int_{z\to 0^-}^{z\to 0^+}\mathbf{J}(z)dz = \frac{eZ_0\dot{n}}{2}\int_{-\infty}^{t} dt_B \left\langle \mathbf{v}(t;t_B,\overline{\theta}_0)\right\rangle_{\overline{\theta}_0}, \tag{3.13}$$

where a change of variables has been made so that the electron birth time t_B is the new time parameter, Z_0 is the impedance of free space, $\dot{n}$ is the number of electrons pumped to the conduction band per unit area per unit time, $\mathbf{v}$ is the electron velocity, and the average is taken over the "birth" phases of the injected electrons. The electron velocity may be expressed in terms of the momentum by using the relation $\mathbf{v}(t;t_B,\overline{\theta_0}) = \mathbf{p}(t;t_B,\overline{\theta_0})/(\gamma(t;t_B,\overline{\theta_0})m')$. From this, the radiation passing through the graphene is altered in a way that can be expressed in terms

of the motion of the electrons within the graphene as governed by the equations of motion for electrons under the original radiation field. In other words, we have a self-consistent set of equations of motion for the coupled electrons and field.

To construct the linear model solution to these equations in [20], the momentum magnitude and direction is decomposed into the unperturbed and the perturbation:

$$p\left(t-t_B\right)=p_0\left(t-t_B\right)+p_1\left(t-t_B\right), \tag{3.14}$$

and

$$\Delta\overline{\theta}\left(t-t_B\right)=\Delta\overline{\theta}_0\left(t-t_B\right)+\Delta\overline{\theta}_1\left(t-t_B\right). \tag{3.15}$$

Then, these forms are substituted into the equations (3.9) and (3.10), and this allows the unperturbed (no THz wave, $\hat{E}=0$) equations to be solved, arriving at a closed-form solution:

$$p_0\left(t-t_B\right)=p_i e^{-(t-t_B)/\tau}, \tag{3.16}$$

and

$$\Delta\overline{\theta}_0\left(t-t_B\right)=\int_{t_B}^{t}dt'\left(\frac{\omega_{_L}}{\gamma_0\left(t'\right)}-\omega\right)=\left(\omega_{_L}-\omega\right)\left(t-t_B\right)-\omega_{_L}\tau ln\left(\frac{\gamma_i+1}{\gamma_0\left(t\right)+1}\right), \tag{3.17}$$

and

$$\gamma_0\left(t-t_B\right)=\sqrt{1+\frac{p_0^2\left(t-t_B\right)}{m'^2c'^2}}, \tag{3.18}$$

is the relativistic factor of an electron as it slows down, and

$$\gamma_i = \sqrt{1 + \frac{p_i^2}{m'^2 c'^2}} = \gamma_0 \left(t = t_B\right), \tag{3.19}$$

is the initial relativistic factor.

Using this solution, lowest-order perturbation theory may be applied, with the electric field of the THz wave as the perturbation. In the linear regime, that is, when the THz radiation field is not too strong, the gain on a single pass through graphene, neglecting cavity losses, is given by

$$\frac{\Delta \hat{E}}{\hat{E}} = R\left(G - L\right), \tag{3.20}$$

where

$$R = \frac{e^2 Z_0 \dot{n} \tau^2 c'^2}{4E_i}, \tag{3.21}$$

is the dimensionless pumping rate,

$$E_i = \gamma_i m' c'^2, \tag{3.22}$$

is the injected energy, and

$$L = \gamma_i \int_0^\infty \left(\frac{1}{\gamma_0^3} + \frac{e^{-\hat{t}/\tau}}{\gamma_0}\right) \frac{\tau_A(\hat{t}) e^{-i\Delta\overline{\theta}_0(\hat{t})}}{\tau^2} d\hat{t}, \tag{3.23}$$

is a loss term representing absorption of THz by the energetic electrons. The quantity

$$G = -\gamma_i \int_0^\infty \frac{ip_0}{\tau^2 \gamma_0} \int_0^{\hat{t}} dt' \left(\frac{\omega_L}{\gamma_0^2} \frac{d\gamma_0}{dp_0} \right) \tau_A(t') e^{-i\Delta\bar{\theta}_0(\hat{t})} d\hat{t}, \tag{3.24}$$

is a potential gain term due to gyrophase bunching that allows the THz fields to be amplified. The real part of Eq. (3.20) describes the change in the magnitude of the electric field, while the imaginary part describes the change in phase. The change in angle due to the radiation field is given by Eq. (2.32),

$$\Delta\hat{\bar{\theta}}_1(t - t_B) = e\hat{E} \left[\int_{t_B}^t dt' \left(\frac{\omega_L}{\gamma_0^2} \frac{d\gamma_0}{dp_0} \tau_A(t' - t_B) \right) - \frac{i}{p_i} \tau_A(t - t_B) \right], \tag{3.25}$$

where

$$\tau_A(t) = e^{-t/\tau} \int_0^t dt' e^{t'/\tau + i\Delta\bar{\theta}_0(t')}. \tag{3.26}$$

We estimate the electric field value at which the gain saturates as follows. Saturation will occur when the angle $\Delta\theta_1$ in (3.25) approaches unity. For simplicity, we take the limit $\gamma_0^{-1}, m' \to 0$. We normalize time in Eqs. (3.25) and (3.26) to the slowing down time τ. We assume the exponent in (3.26) is of order unity, and estimate $\tau_A \sim \tau$. This leads to an estimate for the angle $\Delta\theta_1 \sim e\hat{E}\tau^2\omega_i/(\gamma_i m' c') \equiv \hat{E}/E_c$, where

$$\hat{E}_c = \omega E_i (\omega_i \tau)^{-2} (ec')^{-1} = 6.3 \times 10^6 (\omega_i \tau)^{-2} f[THz] E_i[eV][V/m] \tag{3.27}$$

represents a critical field strength. We note that we previously found gain for sufficiently large slowing down times, $\omega_i\tau$ = 15-20. Thus, for the case of f = 4 THz,

$E_i = 500meV$, $\omega_i\tau = 20$,we obtain a critical field $E_c = 3.2 \times 10^4 V/m$, corresponding to an intensity $I \approx 300W/cm^2$. Of course this is a rough estimate and the true dependence of gain on intensity is determined by solving the nonlinear system as we do in the next section.

Each conduction electron with velocity $\mathbf{v}(t; t_B, \overline{\theta_0}) = \mathbf{p}(t; t_B, \overline{\theta_0})/(\gamma(t; t_B, \overline{\theta_0})m')$ and birth time $t_B < t$, will contribute to the current density [20]. This current density gives rise to a change in the Terahertz radiation field as the radiation passes through the graphene (see Eq. (3.13) of this paper and the accompanying discussion.) The current density acts a source for the field and modifies the field between the m^{th} pass of the THz radiation through the graphene and its $m + 1^{st}$ pass. We assume that the change in field amplitude on each pass/bounce is small. In this case the time dependance of the electric field amplitude $\hat{E}$ will be nearly periodic with period $T_l = l/c$ where l is the path length between passes of the THz through the graphene. We then introduce a time variable t' to represent this rapid, periodic time dependance and use the bounce number, m, to label the slow time dependence. The electric field change upon passing through the graphene once can be cast in terms of the velocity of electrons as

$$\Delta \overrightarrow{E}(t') \equiv E_{m+1}(t') - E_m(t') = \frac{eZ_0\overline{n_0}}{2} \langle \{ \overrightarrow{v}(t') \} \rangle , \tag{3.28}$$

where $Z_0 = 376.73\ \Omega$ is the impedance of free space, e is the elementary charge , $\overline{n_0}$ is the excited electron number density, m is the "bounce number" of THz pulse or continuous wave, that is, how many times THz radiation has passed through

graphene, and the triangular brackets denote the average over the *electrons*.

3.3 Numerical Simulation

To keep computation manageable and limit noise, electrons in the simulation, which follow the equations of motion (Equations (3.4) and (3.5)), are removed from the calculation after a time $\psi \equiv 0.9T_l$ from their injection, by which time they have lost enough energy to be far out of resonance with the THz field. Each removed electron is immediately replaced by a freshly injected electron. The injection rate $\dot{n}$ thus relates to the excited electron number density $\overline{n_0}$ by the relation $\dot{n} = \overline{n_0}/\psi$. The electric field equation now can be written

$$\Delta\overrightarrow{E}(t') \equiv E_{m+1}(t') - E_m(t') = \frac{eZ_0\overline{n_0}}{2}\left\langle\{\overrightarrow{v}(t')\}\right\rangle = \frac{eZ_0(\dot{n}\psi)}{2}\left\langle\{\overrightarrow{v}(t')\}\right\rangle. \quad (3.29)$$

Note that $\hat{E}$ is defined by Eq. (3.8) and thus

$$\Delta\hat{E}(t') = e^{i\omega t}\frac{eZ_0(\dot{n}\psi)}{4}\left\langle\{v_x(t') - iv_y(t')\}\right\rangle, \quad (3.30)$$

where ψ is the effective electron residence time,

or

$$\Delta\hat{E}(t') = e^{i\omega t}\frac{eZ_0(\dot{n}\psi)}{4}\left\langle\{p_x(t') - ip_y(t')\}/(\gamma(t')m')\right\rangle, \quad (3.31)$$

where $p_x - ip_y = pe^{-i\theta} = pe^{-i(\bar{\theta}+\omega t+\phi_0)}$ and

$$\gamma(t) \equiv \sqrt{1 + \left(\frac{p(t)}{m'c'}\right)^2}. \tag{3.32}$$

We use 12950 values for t' (with successive values separated by a time step of $5 \times 10^{-16} s$) and initialize 188 electrons with uniform phase distribution. The field iteration equation is

$$\Delta \mathbf{E} = \Delta \overrightarrow{E}(t') \equiv E_{m+1}(t') - E_m(t') = \frac{eZ_0 \dot{n}}{2} \int_{-\infty}^{t'} dt_B \left\langle \mathbf{v}(t'; t_B, \overline{\theta}_0) \right\rangle_{\overline{\theta_0}}. \tag{3.33}$$

In the simulation, the electric field for $m = 0$ is taken to be low amplitude random noise. $\hat{E}_m$ has a time argument t' and is periodic in t' with period T_l. For each t' particles are launched with a uniform distribution of gyro phases. Particles are thus labeled by 1) their gyro phase, 2) their initial $t' = t'_0$, and 3) their time since birth $t - t_B$. Electron entrance times and entrance phase angles $\overline{\theta}_0$ are uniformly distributed and uncorrelated (that is, uniformly distributed throughout the space of entrance times and phase angles). All electrons begin with the momentum having a magnitude p_i. If a total of N simulation electrons are initialized in a time interval $T_l = l/c$ (where l is the separation between mirrors), then we simply use the discrete equation

$$\Delta \overrightarrow{E}(t') = \left(\frac{eZ_0 \dot{n} \psi}{2}\right) \frac{1}{N} \sum_{particles} \overrightarrow{v}(t'; t_B, \overline{\theta}_0). \tag{3.34}$$

But this only covers the modification of the THz radiation by the graphene's conduction electrons, and does not account for the cavity losses due to mirror absorption,

mirror transmission, or intrinsic (valence electron) graphene absorption. To account for this, before feeding the modified field back into the simulation for the next iteration, the simulated field must first be subject to losses. The losses are treated as a single loss which is a dispersionless, frequency independent loss. It is implemented via the form

$$\overrightarrow{E}(t) \rightarrow \sqrt{1-\zeta}\overrightarrow{E}(t), \tag{3.35}$$

where ζ is the total half-round-trip cavity loss factor which obeys Eq. (3.2).

The simulation works by using the field $E(t')$ from the m^{th} pulse-bounce to compute (using the forward Euler method with time step $\Delta t = (3.3 \times 10^{-4})\tau$ on each iteration) the electron trajectories using Equations (3.4) and (3.5), and then the corresponding electron velocities are used to calculate the field increment using equation (3.29). The field is then incremented to the $E(t')$ for the $m + 1^{st}$ bounce and subject to the cavity loss using equation (3.35). This is repeated until m reaches a pre-set maximum value.

The predictions from the linear model in [20] are an estimation of the single-pass gain ($G - L$ will be referred to as simply "gain") experienced by a THz pulse consisting of only a single frequency. To find numerical results to compare with the linear model, a monochromatic field is injected into the simulation and run through the graphene only once (single pass), and the field is recomputed. The Fast Fourier transform is then computed, in order to isolate the gain of the frequency component in question. In Fig. 3.2, the resulting gain, plotted as a function of frequency, is

shown compared with the linear model. $\omega_i \tau = 61.6$ here.

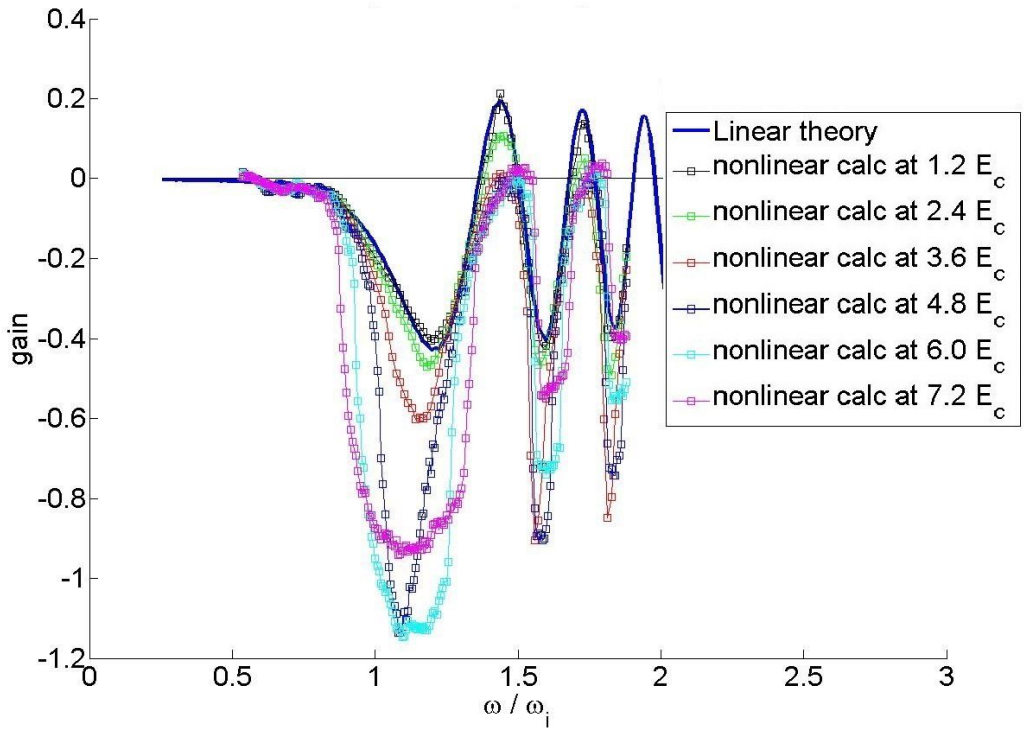

Fig. 3.2: Gain, defined as the $G - L$ from Eq.(3.20), plotted vs. normalized frequency for linear model and numerical result for monochromatic field, single pass, and different electric field strengths expressed as a fraction of the critical field strength (see Eq. 3.27) for nonlinear behavior

These results can also be expressed in terms of the power flux rather than the normalized field strength. Using Eq. (3.27) and the value $\omega_i\tau = 61.6$ we find for the case $E = 2.4E_c$, $P = (1.38 \times 10^7)[f(THz)E_i(eV)]^2 W/m^2$. An enlargement of the region in which the gain as a function of frequency peaks is shown in zoomed-in for in Fig. 3.3 .

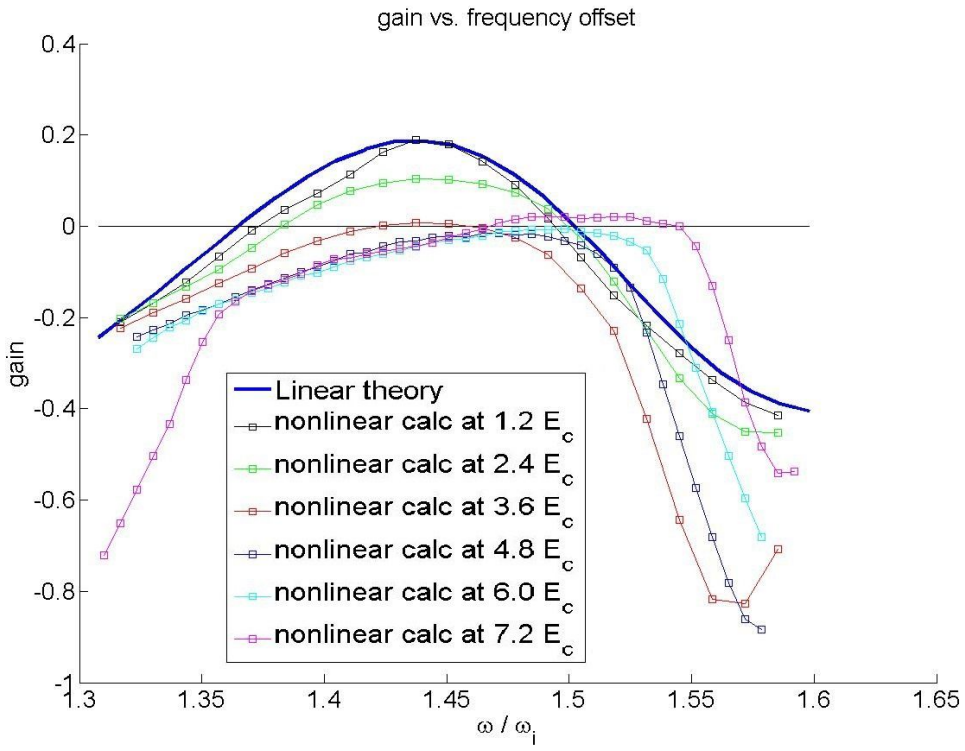

Fig. 3.3: Gain plotted vs. normalized frequency, zoomed in. Curves at same field strengths as in Fig. (3.2).

It can be seen that the gain is roughly halved when $E = 2.4E_c$, and essentially vanishes when $E = 3.6E_c$.

The nonlinear graphene gyrotron theory is expected to reduce to the linear theory in the limit $E << E_c$, but at critical field strengths, the behavior should show reduced gain, as in a conventional gyrotron. The simulation, when integrated forward in this way, confirms this result. This suggests that this parametrization and method of integration provides a useful extension to the linear theory that can be used to estimate what the steady-state operation of the device will look like.

Next, the dynamics for the multi-pass case are considered, and also cavity loss is added, assuming a total cavity loss (half-round-trip) of 4.5 % of energy. Damping time is now 1.5 ps and we are restricting the field to a single frequency by filtering other frequency components out via Fourier transform after each pass. The resulting efficiency plot is shown in Fig. 3.4.

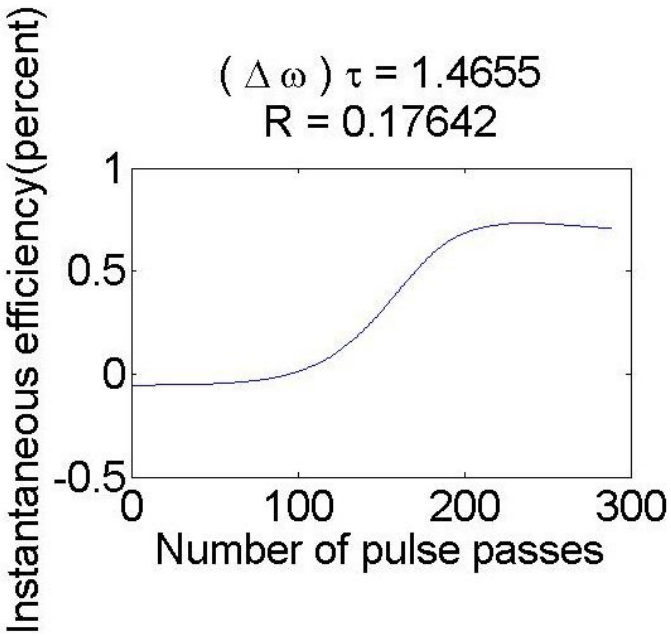

Fig. 3.4: Efficiency ramp up, 288 passes

3.4 Conclusion

The nonlinear theory, evaluated with the integration methods used here, provides a useful extension to the linear theory, and agrees as expected with that theory in the low-field limit as well as displaying physically reasonable saturation behavior. Cavity losses can be incorporated which allow a more realistic consideration of device operation, and efficiencies up to a few tenths of 1% can be feasible, defined as the device output power divided by the power going into pumping of the electrons. Since the absorption of the IR laser pump may be very inefficient, the true whole-

device efficiency may be significantly lower. Nevertheless, the device does coherently oscillate.

3.5 Appendix: Intuitive Understanding of Gain

Here, the goal is to explain, conceptually, why the gain function behaves as it does and what it might mean physically. First, the phase angle given by Eq. (2.23) is shown in Fig. 3.5 as a function of time for two frequencies, 13.0 THz (at which there is a net loss) and at 14.1 THz (at which there is net gain).

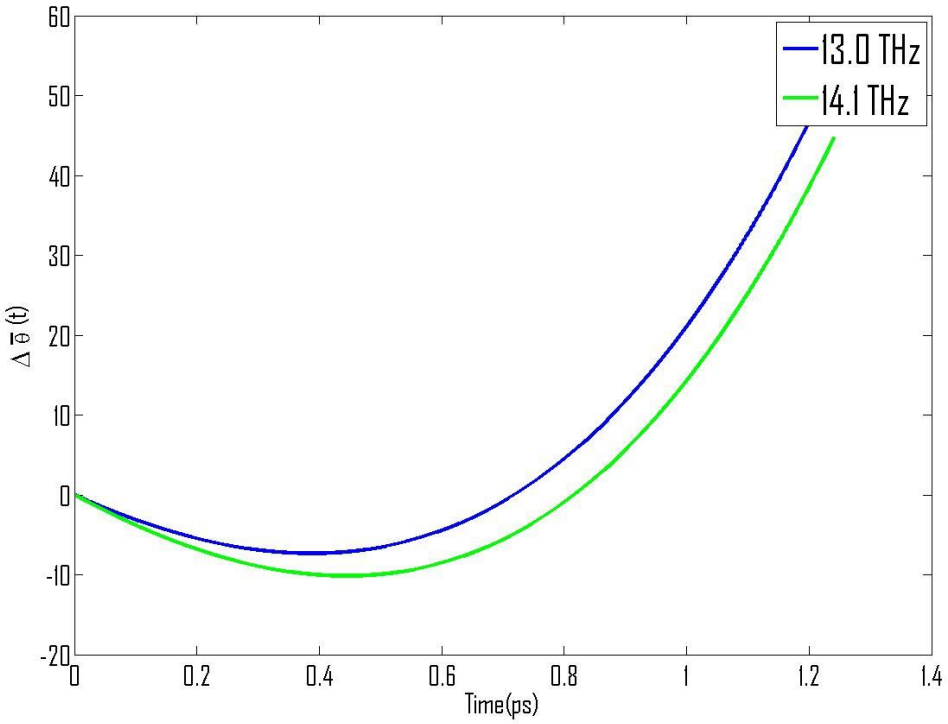

Fig. 3.5: Dynamics:phase angle

Next, is the complex exponential $e^{i\Delta\bar{\theta}(t)}$ in Fig. 3.6. Notice that because the two phase angle functions in Fig. 3.5 bottom out at different phase values, the

complex exponentials behave dramatically differently around the phase-stationary point.

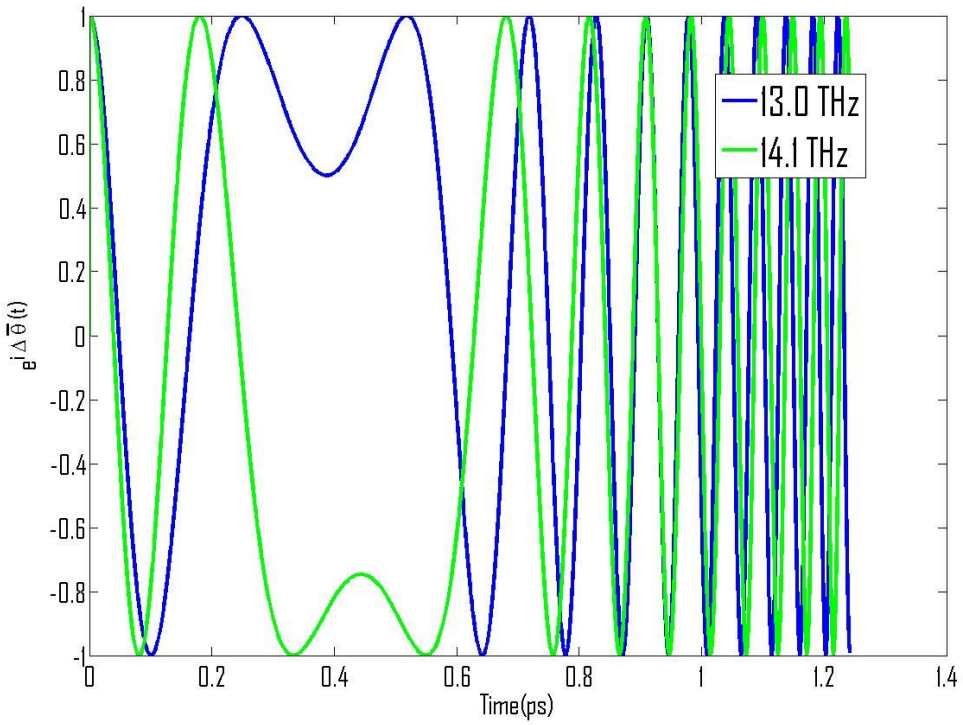

Fig. 3.6: Dynamics: complex exponential $e^{i\Delta\bar{\theta}(t)}$ versus time. Imaginary part excluded.

Then the time integral of the complex exponential is shown in Fig. 3.7. Because of the different behaviors of the complex exponential around the resonant time (phase-stationary time), the integral ends up at dramatically different values at late times for these two frequencies.

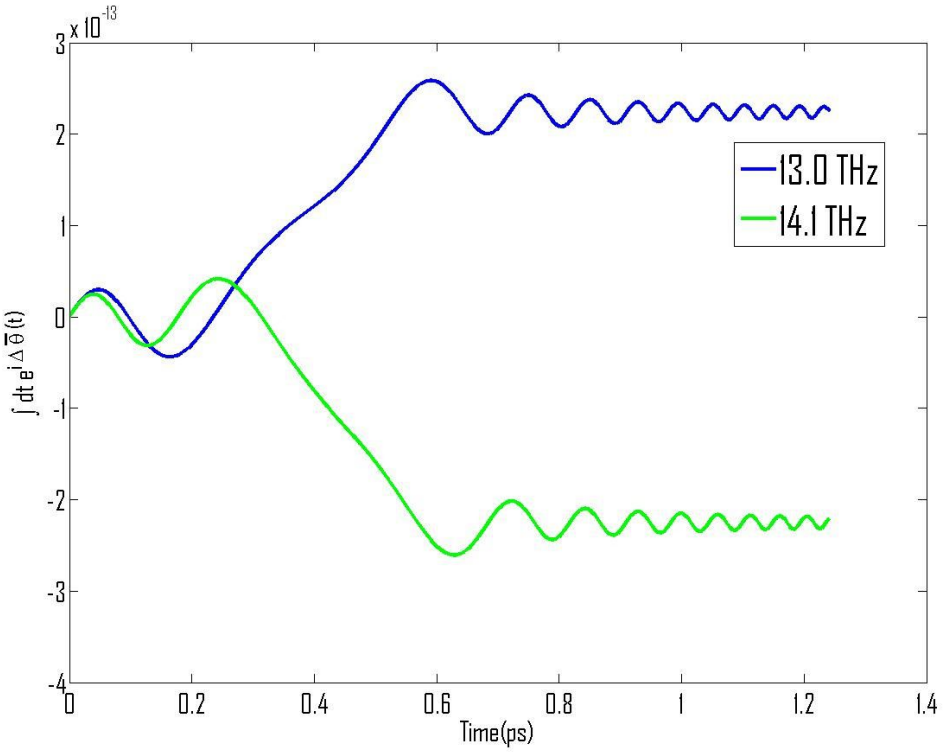

Fig. 3.7: Dynamics: Integral of complex exponential. Imaginary part excluded.

Note that this factor appears explicitly in (A9) as the determining function for the gain. Essentially, what happens is that the stationary phase of gyration of the electrons relative to the field determines whether gain or loss occurs.

Bibliography

[1] Andronov A A 1999 From H. Kroemer and B. Lax to Modern Solid-State (Semiconductor) Cyclotron Resonance Masers *IEEE Transations on Plasma Science* **27**(2) 303-311

[2] Nusinovich G S 2004 *Introduction to the Physics of Gyrotrons* (Baltimore: Johns Hopkins)

[3] Coyne K 2012 Nov 21 Magnets from Mini to Mighty Retrieved from https://nationalmaglab.org/education/magnet-academy/learn-the-basics/stories/magnets-from-mini-to-mighty

[4] Idehara T and Sabchevski S P 2017 Gyrotrons for High-Power Terahertz Science and Technology at FIR UF *J Infrared Milli Terahz Waves* **38** (1) 62-86

[5] Novoselov K S 2005 Two-dimensional gas of massless Dirac fermions in graphene *Nature* **438** 197-200

[6] Aoki H 1986 Novel Landau level laser in the quantum Hall regime *Appl. Phys. Lett.* **48** (9) 559 - 560

[7] Wendler F and Malic E 2015 Towards a tunable graphene-based Landau level laser in the terahertz regime *Scientific Reports* **5** 12646-1 12646-7

[8] Wang Y, Tokman M and Belyanin A 2015 Continuous-wave lasing between Landau levels in graphene *Phys. Rev. A* **91** (3) 033821-1 033821-8

[9] Mittendorff M *et al.* 2015 Carrier dynamics in Landau-quantized graphene featuring strong Auger scattering *Nature Physics* **11** 7581

[10] Morimoto T, Hatsugai Y and Aoki H 2008 Cyclotron radiation and emission in graphene *Phys. Rev. B* **78** (7) 073406-1 - 073406-4

[11] Boubanga-Tombet S, Chan S, Watanabe T, Satou A, Ryzhii V and Otsuji T 2012 Ultrafast carrier dynamics and terahertz emission in optically pumped graphene at room temperature *Phys. Rev. B* **85** (3) 035443-1 - 035443-6

[12] Jago R, Winzer T, Knorr A and Malic E 2015 Graphene as gain medium for broadband lasers *Phys. Rev. B* **92** (8) 085407-1 085407-7

[13] Winzer T, Mali E and Knorr A 2013 Microscopic mechanism for transient population inversion and optical gain in graphene *Phys. Rev. B* **87** (16) 165413-1 165413-4

[14] Nusinovich G S, Thumm M K A, and Petelin M I 2014 The Gyrotron at 50: Historical Overview *Journal of Infrared, Millimeter, and Terahertz Waves* **35** (4) 325-381

[15] Du C, Qi X, Kong L, Liu P, Li Z, Xu S, Geng Z and Xiao L 2015 Broadband Tunable Pre-Bunched Electron Cyclotron Maser for Terahertz Application *IEEE Transactions on Terahertz Science and Technology* **5** (2) 236 - 243

[16] Yin L-J *et al.* 2017 Landau quantization of Dirac fermions in graphene and its multilayers *Front. Phys.* **12**(4)

[17] Hongki M (Oct 11, 2006 lecture) Electronic Structure of Graphene Graphene Monolayer Graphene Bilayer. Web. 21 Nov. 2012. <http://www.ph.utexas.edu/ macdgrp/meetings/hongki-monolayer.pdf>.

[18] Zavolsky N A, Zapevalov V E and Moiseev M A 2001 Efficiency Enhancement of the Relativistic Gyrotron *Radiophysics and Quantum Electronics* **44** (4) 318-325

[19] Park J *et al.* 2011 Band gap formation in graphene by in-situ doping *Appl. Phys. Lett.* **98** (20) 203102-1 - 203102-3

[20] Cole N and Antonsen T M 2017 Electron Cyclotron Resonance Gain in the Presence of Collisions *IEEE Transactions on Plasma Science* **45** (11) 2945-2954 © 2017 IEEE. Reproduced under Thesis Policy found online at `https://www.ieee.org/publications_standards/publications/rights/permissions_faq.pdf`(accessed 11/27/2017). Reprinted with permission from authors.

[21] Frogley M D, Dynes J F, Beck M, Faist J and Phillips C C 2006 Gain without inversion in semiconductor nanostructures *Nature Materials* **5** 175-178

[22] Kuzmenko A B, van Heumen E, Carbone F and van der Marel D 2008 Universal Optical Conductance of Graphite *Phys. Rev. Lett.* **100**, (11) 117401-1 117401-4

[23] Hwang E H, Hu B Y and Das Sarma S 2007 Inelastic Carrier Lifetime in Graphene *Phys. Rev. B* **76** (11) 115434-1 115434-6

[24] Winzer T, Knorr A and Malic E 2010 Carrier Multiplication in Graphene *Nano Letters* **10**(12) 4839-4843

[25] Tse W and Das Sarma S 2009 Energy Relaxation of Hot Dirac Fermions in Graphene *Phys. Rev. B* **79** (23) 235406-1 - 235406-5

[26] Mittendorff M *et al.* 2014 Intraband carrier dynamics in Landau-quantized multilayer epitaxial graphene *New Journal of Physics* **16** 123021-1 123021-9

[27] Plochocka P, Kossacki P, Golnik A, Kazimierczuk T, Berger C, de Heer W A and Potemski M 2009 Slowing hot-carrier relaxation in graphene using a magnetic field *Phys. Rev. B* **80** (24) 245415-1 - 245415-5